UCRL 8354

UNIVERSITY OF
CALIFORNIA

Radiation Laboratory

ANGULAR DISTRIBUTION OF PHOTOPIONS FROM HYDROGEN

BERKELEY, CALIFORNIA

UCRL-8354
Physics and Mathematics

UNIVERSITY OF CALIFORNIA
Radiation Laboratory
Berkeley, California

Contract No. W-7405-eng-48

ANGULAR DISTRIBUTION OF PHOTOPIONS FROM HYDROGEN

Edward A. Knapp
(Thesis)

July 1, 1958

Printed for the U. S. Atomic Energy Commission

ANGULAR DISTRIBUTION OF PHOTOPIONS FROM HYDROGEN

Contents

ANGULAR DISTRIBUTION OF PHOTOPIONS FROM HYDROGEN

Edward A. Knapp

Radiation Laboratory
University of California
Berkeley, California

July 1, 1958

ABSTRACT

An accurate measurement of the differential cross section for the photoproduction of positive pions has been made at the Berkeley synchrotron, for photon energies of 260 and 290 Mev. The mesons were produced in a thin-walled liquid hydrogen target, and the meson-detection apparatus utilized the characteristic $\pi - \mu$ decay of the meson. The measurements were done in two steps, from 0° to 50° with equipment specifically designed to reduce a very high positron background, and from 30° to 160° with equipment whose efficiency and solid angle could be accurately determined.

The experimental results in the small-angle region definitely show the effects of "photoelectric" production of pions from the cloud surrounding the nucleon, which are characterized by an abrupt flattening of the cross section in the region forward of 40° (c.m.). The results are compared to the theory of photoproduction derived from the dispersion relations, and the agreement is satisfactory within the limitations of the theory.

I. INTRODUCTION

The photoproduction of positive pions from hydrogen is one of the fundamental reactions encountered in the study of pi-meson phenomona, and as such has been investigated quite extensively wherever high-energy photon beams have been available.[1-10] Recently, however, with the advent of more refined theories describing the photopion interaction,[11, 12] there has been a revival of interest in the measurement of the reaction, for the existing data are insufficient to confirm some of the finer details of these theories.

Very little experimental information has hitherto been available on the angular distribution of this reaction in the angular region from 0° to 40°, where it is more difficult to make accurate measurements owing to the high electron background present. Furthermore, the existing data over the remaining angular range were neither internally consistent between the various laboratories nor statistically accurate enough to enable a critical selection between the various forms of the theories to be made.

With this in mind the measurement of the differential cross-section was undertaken, with the dual aims of obtaining data in the region forward of 40° (c.m.), and of materially reducing the errors associated with the values of the cross section over the angular interval from 40° to 160°. Our measurements were made in two steps; from 50° to 0^{0} (c.m.) with equipment specifically designed to reduce the background, and from 30° to 160° with more conventional apparatus, allowing enough overlap for careful normalization.

Similar experiments on the forward-angle region have been completed or are nearing completion by Lazarus[14] at Stanford University and by Malmberg and Robinson[15] at the University of Illinois. These experiments (performed at different energies and by different techniques) show essentially the same behavior as the results reported here.

II. EXPERIMENTAL ARRANGEMENT

A. General Experimental Method

A target containing liquid hydrogen was bombarded with the 340-Mev bremsstrahlung beam from the Berkeley synchrotron, and the mesons produced were counted as a function of angle for photon energies of 260 Mev and 290 Mev. The small-angle arrangement was designed specifically to reduce the positron background, and in both cases the mesons were detected by requiring them to exhibit their characteristic $\pi - \mu$ decay, their energy being determined by their range.

1. Small-Angle Arrangement

The layout in the synchrotron magnet room is shown in Fig. 1. The synchrotron spread-out beam was used with a beam-pulse duration of 4 milliseconds. The beam passed through a thin-walled ion chamber, through two lead collimators, through a sweeping magnet, through the target, and finally into a thick-walled ion chamber of the type originated at Cornell. The target vacuum system extends through the sweeping magnet so that the only source of background positrons is the target itself. Mesons produced in the target are deflected away from the direct photon beam by a magnetic field, and are required to pass through a lead scatterer placed halfway down the magnetic channel. This serves to remove a large fraction of the positrons deflected with the mesons, and makes the experiment feasible at the small angles.

The counter telescope requires a particle making a valid count to stop in the fifth counter and decay between 3×10^{-8} and 9×10^{-8} seconds after coming to rest. The momentum width of the magnetic channel is quite broad compared with the energy interval determined by the range of the particle, so that the energy is completely determined by the amount of absorber placed in front of the telescope. Angles are varied in this arrangement by rotating the whole magnet-telescope system about the center of the target.

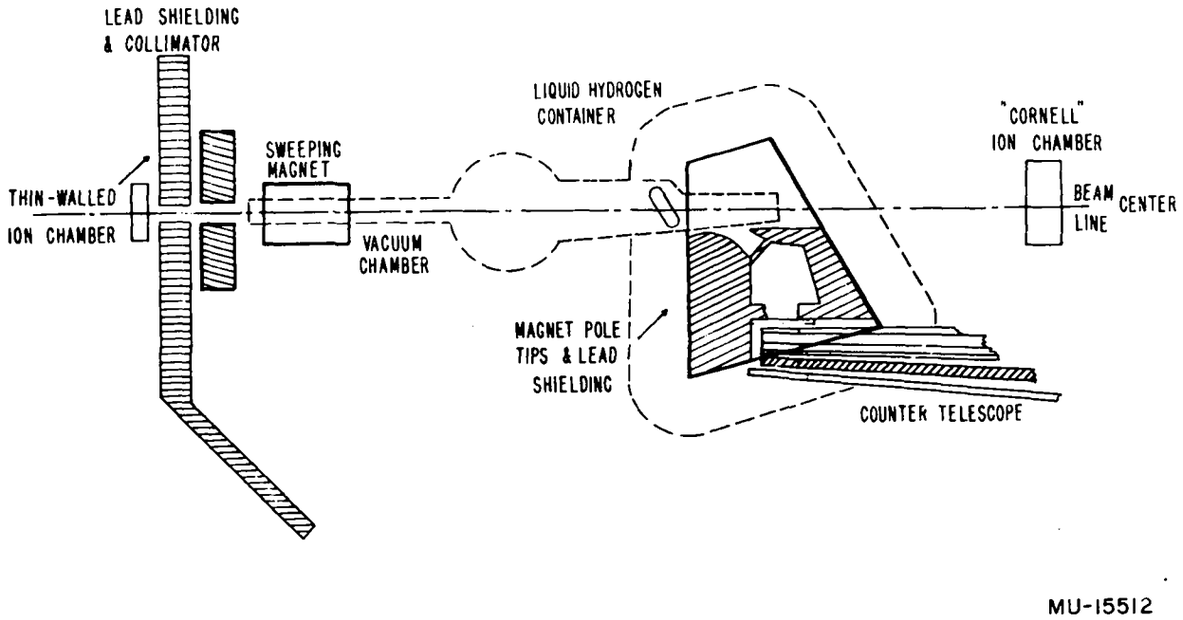

Fig. 1. Arrangement of experimental apparatus for small-angle measurements.

2. Arrangement for Wide Angles

The setup for measurements from 30° to 160° is shown in Fig. 2. The arrangement is similar to that in the small-angle measurements; however, the mesons are not deflected by a magnet, but pass directly into the telescope. Since the positron background is small in this case, no lead scatterer was required. The telescope rotates about the center of the target volume.

B. Meson Detection

1. Electronics

The basis of the identification of the positive pions in this experiment was their characteristic mean life of 2.54×10^{-8} second. This general method of meson detection was originated by Chamberlain, Mozley, Steinberger, and Wiegand, [16] and has been utilized extensively in the past. The electronic equipment used in this experiment has been more fully described by Imhof, Kalibjian, and Perez-Mendez. [17]

A simple block diagram of the π - μ electronics is shown in Fig. 3. When the correct combination of coincidence and anticoincidence pulses is registered in the multiple coincidence-anticoincidence unit, a gate is formed by the gate generator. The requirements of this coincidence may be varied to suit the particular problem at hand. Our specific requirements are discussed in the description of the counter telescopes. The length of this gate is 6×10^{-8} second, and it is made to arrive at a second coincidence circuit, in coincidence with the stopping scintillator, at a 3×10^{-8}-second delay relative to the pulse of the stopping π meson. Thus a π meson of the correct energy which has come to rest in the stopping counter is registered in Coincidence 1 if it decays between 3×10^{-8} and 9×10^{-8} second after coming to rest.

It is also possible for two particles to pass through the counter between 3×10^{-8} and 9×10^{-8} second apart, or for a μ - e decay to take place in this interval, thus appearing like a π meson. These

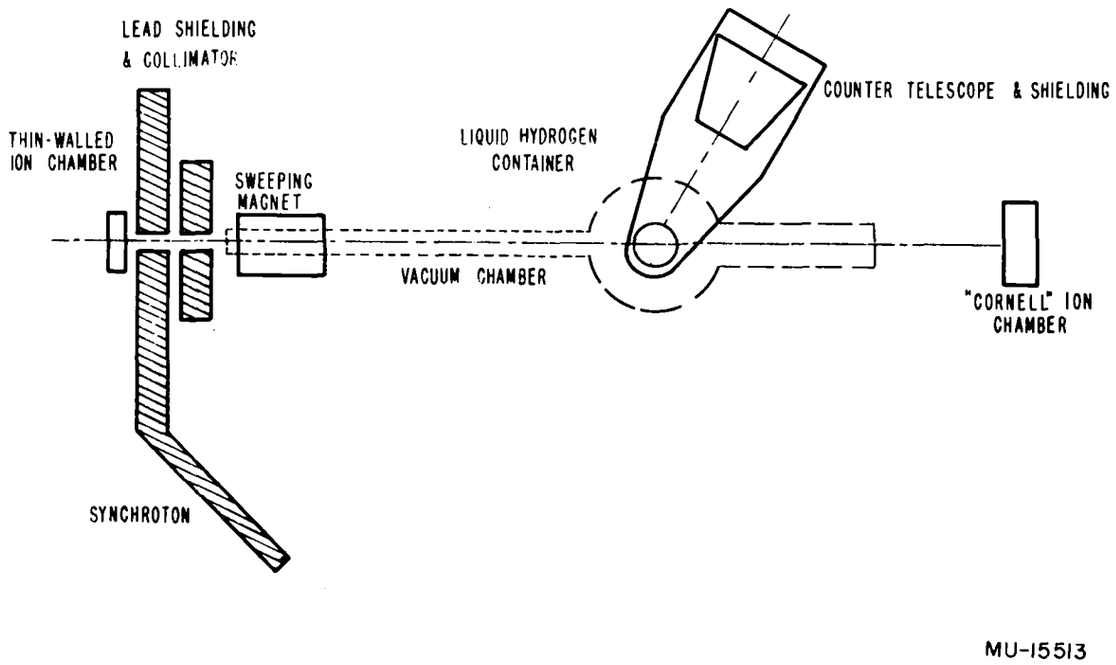

Fig. 2. Arrangement of experimental apparatus for wide-angle measurements.

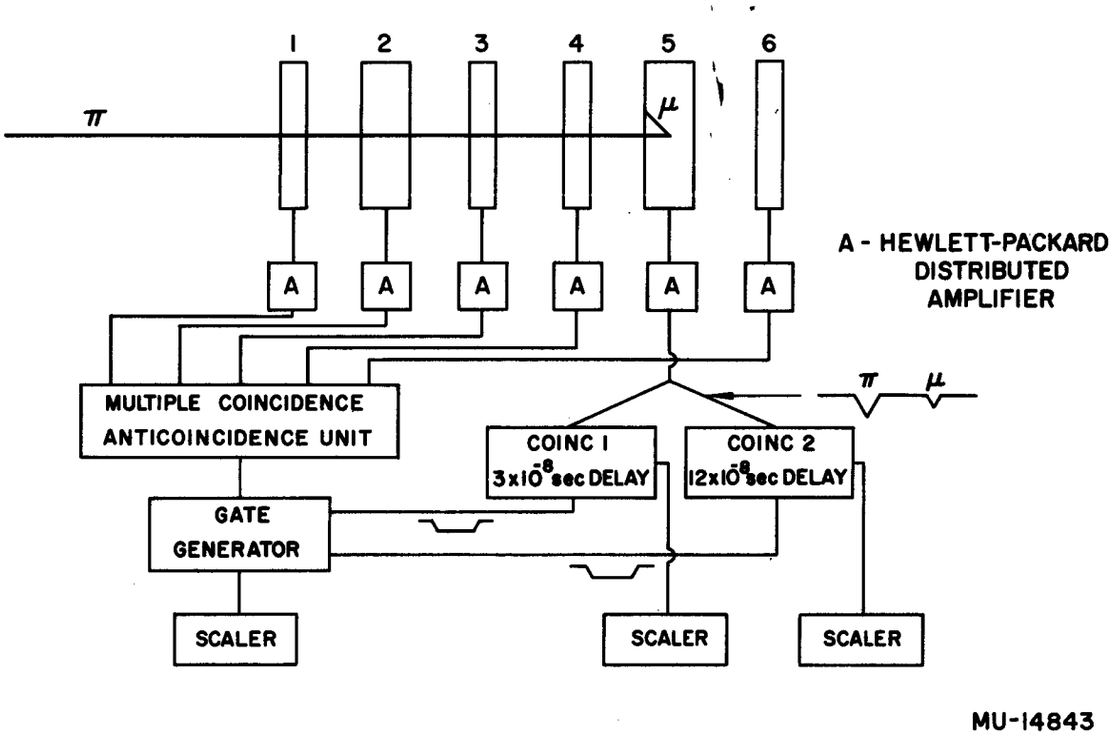

Fig. 3. Block diagram of $\pi - \mu$ electronics.

cases were monitored with a gate to another coincidence unit, Coincidence 2, delayed by 16×10^{-8} second relative to the stopping pulse. At this delay 99.8% of the π mesons will have decayed, so that the coincidences recorded are a good measure of the spurious counts in the first coincidence unit.

The signals are taken from photomultiplier tubes viewing the scintillators and amplified in Hewlett-Packard 460-A distributed amplifiers, for the coincidence circuits all require a pulse height of 4 volts for optimum operation. The multiple coincidence-anti-coincidence unit utilized to trigger the gate generator had two anti-coincidence and three coincidence inputs which could be switched in any combination, making it useful with many combinations of counters in the telescope. This circuit was designed by Evans[18] and is standard equipment at the Radiation Laboratory; it has a resolving time of about 1×10^{-8} second. The pulse from the Evans coincidence unit is amplified and inverted by a Hewlett-Packard 460-B amplifier and is then connected to the gate generator.

The gate generator has also been described in detail in the paper by Imhof, Kalibjian, and Perez-Mendez.[17] A schematic diagram of the gate generator is shown in Fig. 4. The rise time of the gate is about 5×10^{-9} second, and its amplitude is 4 volts. The duration of the gate is set by a length of shorted coaxial cable, here set to be 6×10^{-8} second. This particular circuit has proven extremely stable, and has shown no appreciable drifts in the course of the experimental work.

The time delay of the gates to the coincidence circuits No. 1 and No. 2 is obtained by requiring them to travel through different lengths of RG 63/U cable. The second coincidence circuits are of the crystal diode type. A schematic diagram of these is shown in Fig. 5. The operation of these circuits is optimum at input pulses of from 2 to 5 volts, and in this range the singles-to-doubles ratio is about 12 to 1, measured with a mercury pulser. Since the Hewlett-Packard

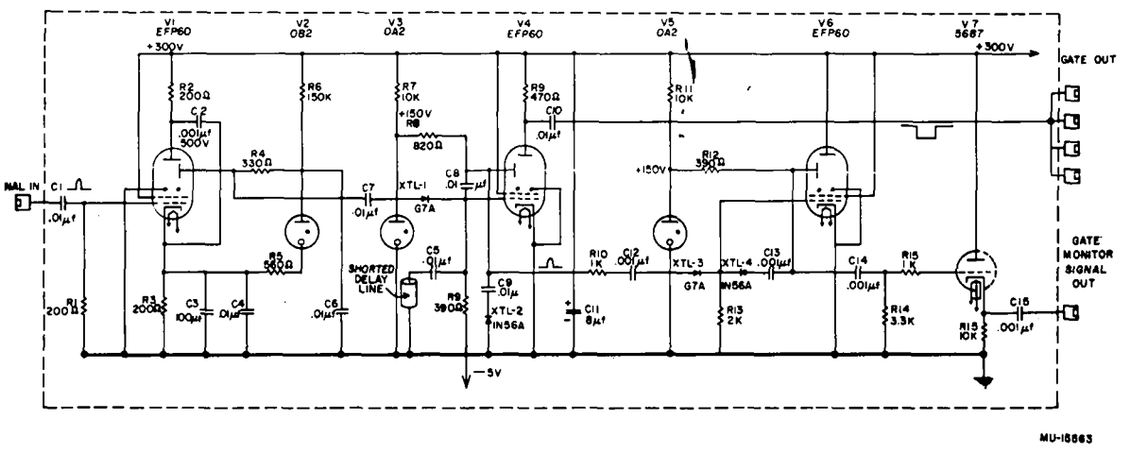

Fig. 4. Circuit diagram for gate generator.

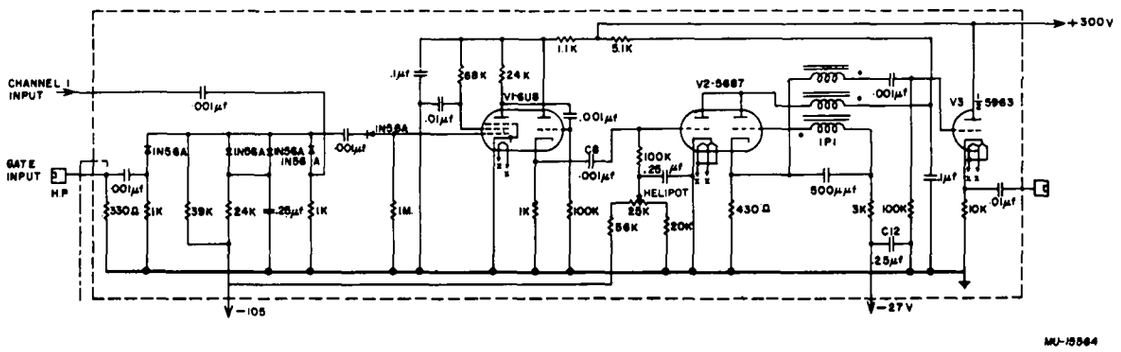

Fig. 5. Circuit diagram for crystal diode coincidence circuits.

amplifiers limit pulse height at about 8 volts, it is impossible to feed through single pulses from the stopping scintillator.

During operation it is important to have the discrimination level of the two coincidence circuits set at the same value. This level is controlled by varying the grid bias on the 5687 tube, which acts as a blocking oscillator producing a pulse for a standard UCRL 1024 scaler. During the experiment this discrimination level is checked by feeding pulses into the gate generator from a 100-kilocycle pulser and balancing the number of accidental coincidences from the two coincidence circuits; this periodic check was done once daily during the course of the experimental measurements.

In order to monitor the stability of the equipment, small Ru^{106}-Rh^{106} sources were attached to the scintillators, and the number of single pulses per minute was recorded each morning and evening for each scintillator. This was accomplished by counting the number of gates produced in one minute with the multiple coincidence-anticoincidence unit switched to count single pulses. This checked all the electronics through the gate generator and allowed any drifts to be compensated by changing the photomultiplier high voltages. The only drifts noted were in the gain of the Hewlett-Packard amplifiers, and these were small.

The validity of our detection scheme may be shown in a variety of ways:

(a) A plateau was observed in the counting rate as a function of the high voltage on the stopping scintillator. A typical plateau is shown in Fig. 6.

(b) A plateau was observed in the meson counting rate as a function of the high voltage on the scintillators triggering the gate circuit. A typical plateau is shown in Fig. 7.

(c) By varying the delay of the gate relative to the stopping pulse, it is possible to measure the mean life of the particles we are observing. The mean lives measured agree within statistics with the

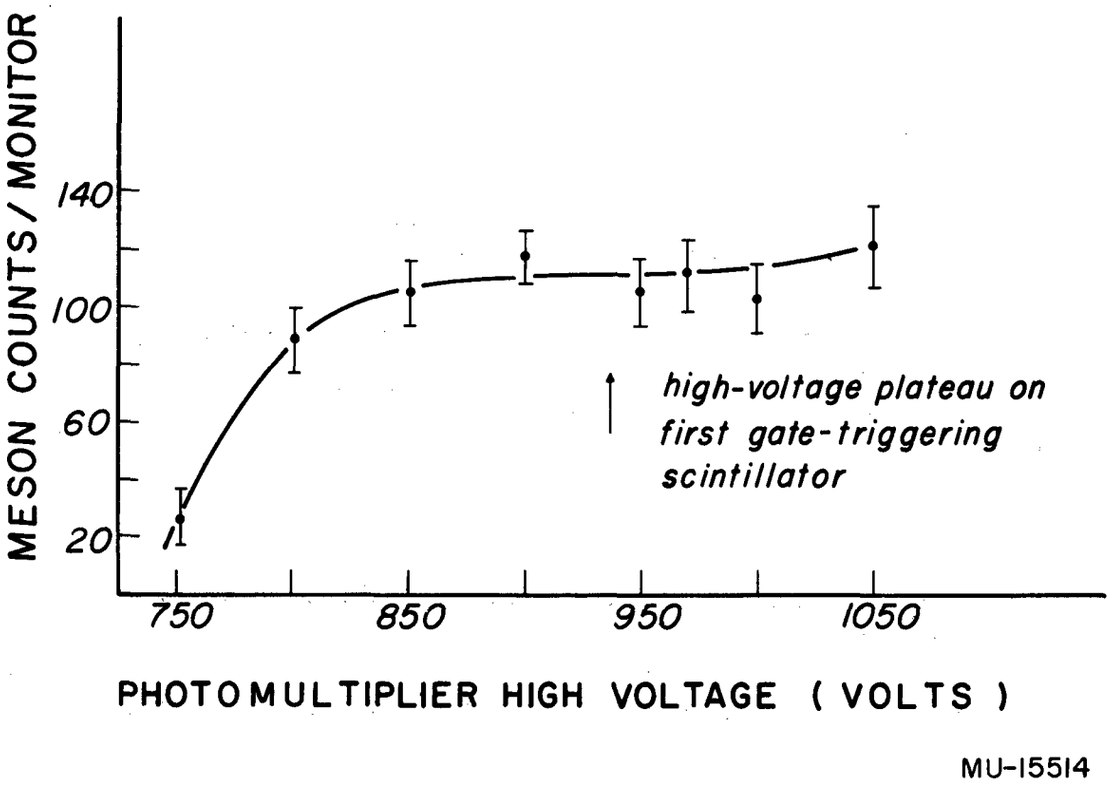

Fig. 6. High-voltage plateau on stopping scintillator.

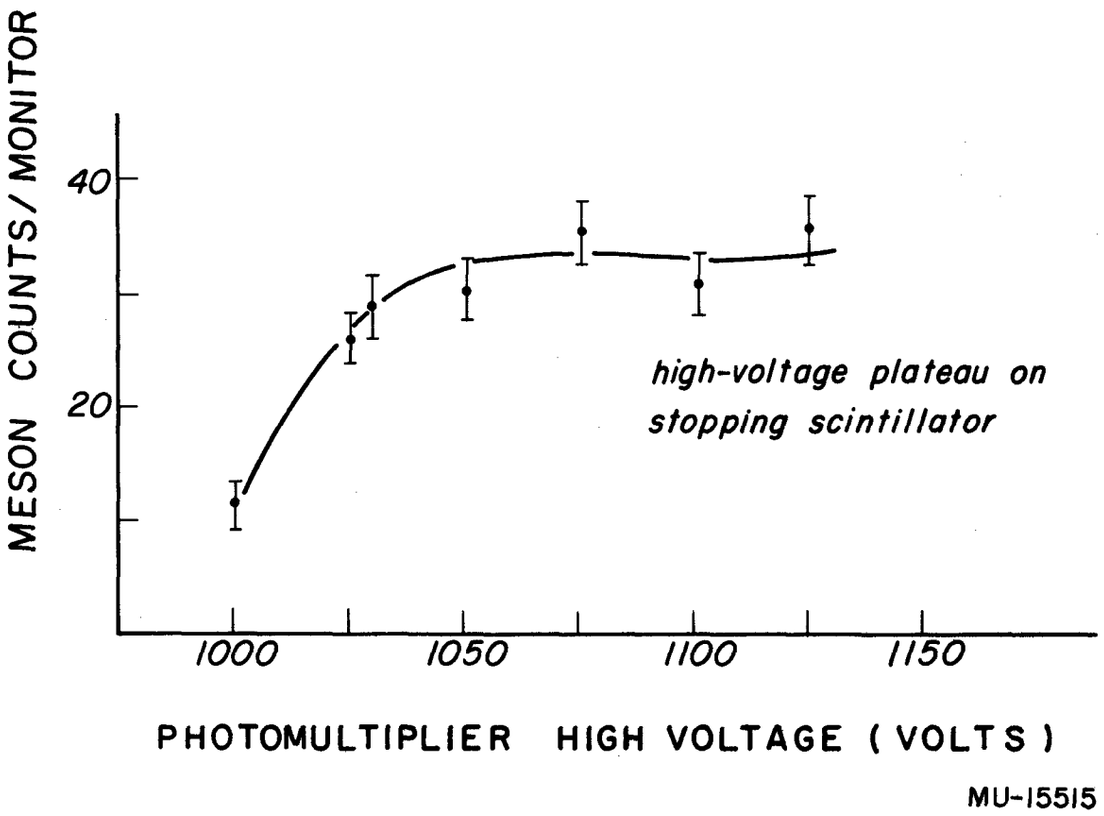

Fig. 7. High-voltage plateau on first gate-triggering scintillator.

accepted value of 2.54×10^{-8} second.[19] A typical mean-life curve taken at the synchrotron is shown in Fig. 8.

(d) The telescope operation was checked in a "pure" π-meson beam at the cyclotron, and its operational characteristics were found to be the same as encountered at the synchrotron. (See Appendix.)

2. Counter Telescopes and Channels

a. Arrangement for small angles

The channel and telescope used in the small-angle measurements is shown in Fig. 9. The mesons are produced in the liquid hydrogen target, where the target's angle of inclination to the beam was chosen so that the variation in cross-sectional area of the irradiated portion was minimum as the angles were changed. Flat parallel sides were used to minimize any alignment error.

The 340-Mev synchrotron pair-spectrometer magnet was used to provide the magnetic field. This magnet has a gap of $3\frac{1}{2}$ inches, with a maximum field of 16 kilogauss. The positive mesons were deflected in this field and were incident upon a lead scatterer-converter placed as shown in Fig. 9. The thickness of this lead was chosen to minimize the positron flux at the telescope while keeping the loss of mesons due to multiple Coulomb scattering as small as possible. For the 260-Mev photons, 1.5 centimeters of lead was chosen. This presents 2.75 radiation lengths to the positrons, which is sufficient to reduce the number of background particles triggering the gate generator by a factor of about 100 at the 0° angle, where this background problem was worst.

For 290-Mev photons the mean squared multiple-scattering angle was smaller and there were less stringent requirements due to the total range of the particle, so that a thicker piece, 2.50 cm, was used. This reduced the positron background at the telescope by a factor of 400.

The $\pi - \mu$ telescope required a triple coincidence (1, 3, and 4) to trigger the gate generator. Counters 2 and 6 were placed in

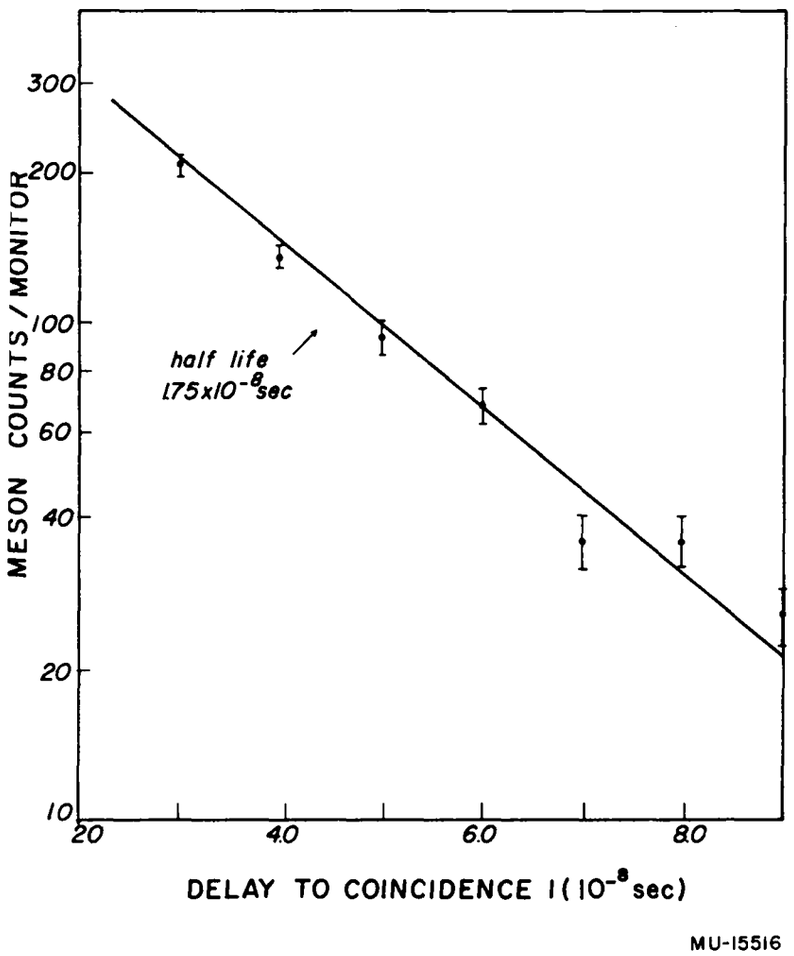

Fig. 8. Half-life curve taken at synchrotron.

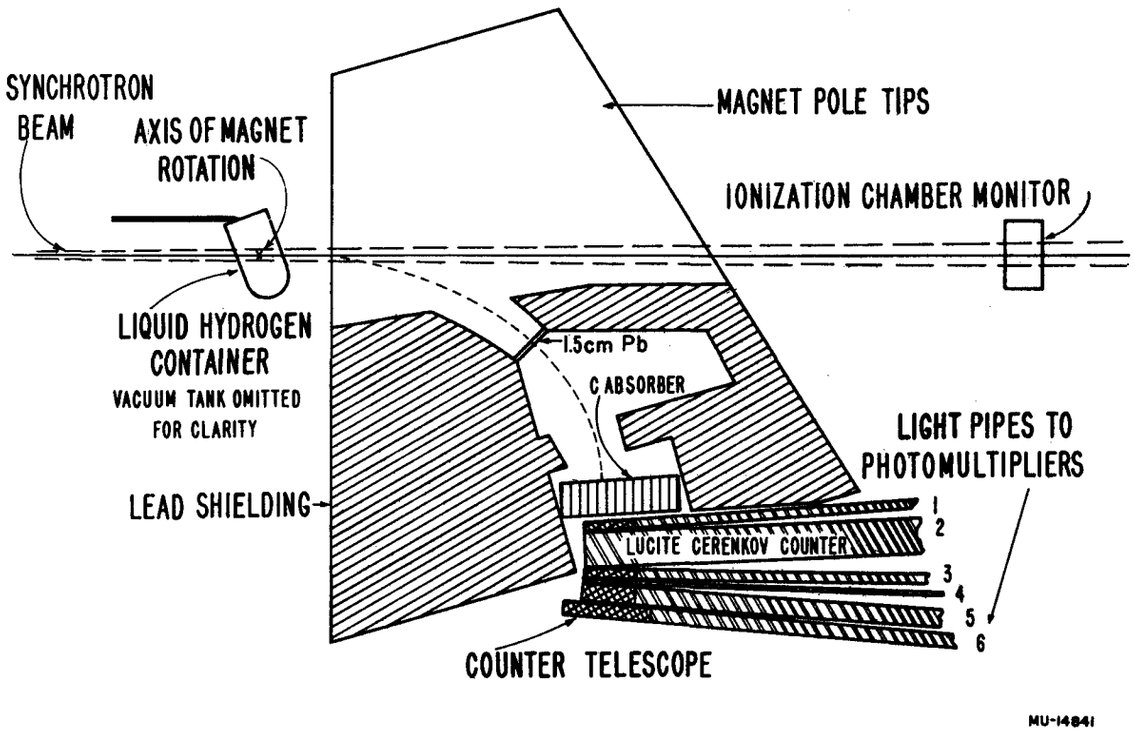

Fig. 9. Magnet and counter-telescope arrangement used in the angular range from 0^{o} to 50^{o}.

anticoincidence. Counter No. 2 is a Cherenkov counter viewed with two RCA 6810 photomultiplier tubes whose outputs are added. The sensitive area is made of Plexiglas, which has an index of refraction of 1.49, and is 2 inches thick. Thus any particle passing through the counter with a velocity greater than 0.67 c produces a pulse, and hence a coincidence is not recorded. To come to rest in the fifth counter a meson enters the Cherenkov counter with a velocity of 0.64 c and thus does not produce a pulse. Positrons and electrons, however, have $\beta \sim 1$ down to quite low energies, and thus are rejected. However, because of poor light-collection efficiency, this counter is not 100% efficient. Counter 6 rejects any particle passing through the entire telescope. Counters 1, 3, and 4, Counter 5 (the stopping scintillator), and Counter 6 are all made of standard UCRL plastic scintillator material. Counter 5 utilized an RCA 6810 photomultiplier. All had 30-inch Plexiglas light pipes to remove the phototubes from the region of high-magnetic-field, and the tubes were also shielded with iron and mu metal against any stray magnetic field.

As the angle of observation was changed, the transformation from center-of-mass system to laboratory system for a constant photon energy required the energy of the observed meson to change. This change was made by changing the amount of absorber in front of the telescope, and by changing the value of the magnetic field. As was remarked, the magnetic field does not determine the pion energy, for the magnetic channel is very broad compared with the ΔE_π accepted by the telescope, but the correct energy still must fall in the center of the channel. The correct magnet setting was obtained with the floating-wire technique. This measurement relies on the fact that a wire under tension with a current flowing through it will assume a position in a magnetic field equivalent to that of a particle orbit, where the momentum of the particle is related to the current and tension in the wire. The sign of the magnetic field was also checked in this way.

b. Arrangement for wide angles

The counter telescope used in the extended-angle measurements is shown in Fig. 10. The mesons are again produced in a liquid hydrogen target, which in this case is a cylinder 3 inches in diameter. The telescope consists of 3 scintillators to trigger the gate generator, a stopping scintillator, and a large scintillator in anticoincidence to reject all particles that pass completely through the telescope. All the scintillators were viewed with RCA 6199 photomultiplier tubes.

The solid angle subtended by this telescope is determined by the area of the front scintillator. The following counters are successively larger in such a way that multiple Coulomb scattering of the mesons in coming to rest may be neglected or easily estimated. This removes one energy-dependent correction from the analysis of the data. The lab energy of the meson is determined by the amount of copper absorber placed between the second and third scintillators. This copper was fitted to an assembly so that it could be repositioned exactly for each run. The whole counter assembly rotated on a cart pivoted about the center of the target, and angles could be set to 0.1° accuracy.

C. Targets

The targets used in this experiment were quite similar for both the small-angle and large-angle arrangements. They consisted of a large reservoir for storage of the liquid hydrogen, and a small target assembly suspended below in the beam line. The space surrounding the hydrogen-filled target and reservoir was evacuated, and the cold parts were shielded from the thermal radiation of the vacuum-tank walls by a copper shield held at liquid nitrogen temperature. The small target assembly could be emptied or filled by closing or opening a valve on the line venting it. Figure 11 shows the reservoir and target arrangement for the small-angle measurements. In this setup the magnet-coil cases required the target to be displaced from under the reservoir, in order to be located close to the magnet pole tips. In the wide-angle setup the cylindrical target was directly under the reservoir.

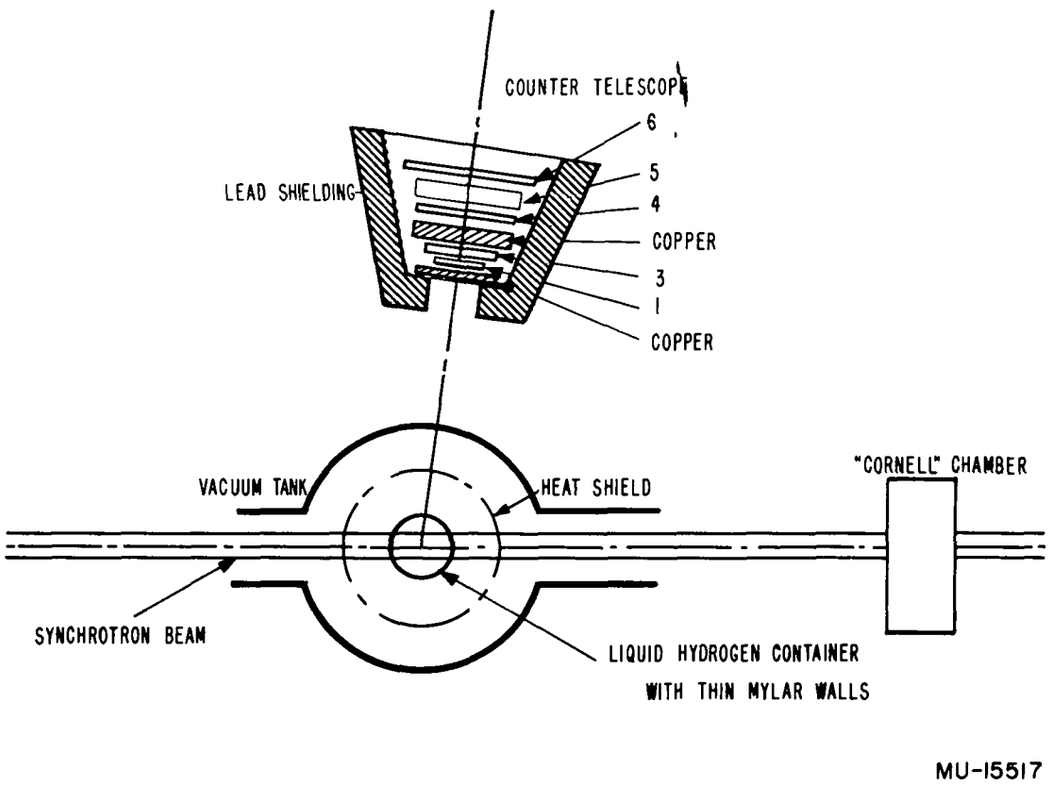

Fig. 10. Target and counter-telescope arrangement used in wide-angle measurements.

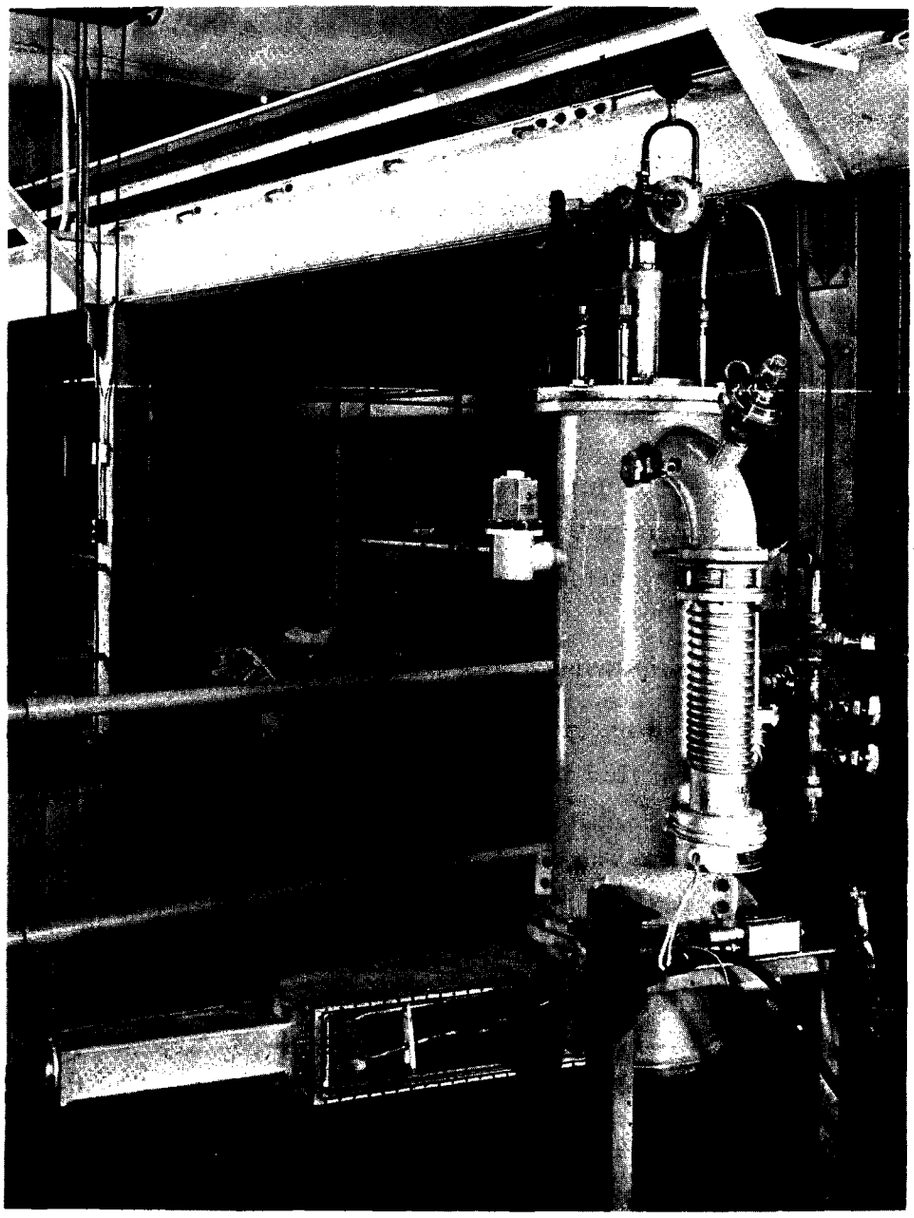

ZN-1979

Fig. 11. Liquid hydrogen target used for small-angle measurements.

The small target containers used in both experiments were of similar construction, although the small-angle target had flat sides and the one used for the wide-angle experiments was cylindrical in shape. The walls of the target were made of 0.005-inch Mylar, which, because of the low Z of this plastic material, contributed very little to the background problem encountered in the measurements. The consumption of hydrogen in most cases was less than 1 liter per hour.

In the small-angle setup, a thin window was provided in the vacuum jacket between the target and the entrance to the magnetic channel to reduce the scattering of the mesons on their way to the detectors. In the wide-angle arrangement, no thin window was required, for the vacuum tank itself was made of relatively thin (3/32-inch) aluminum tubing, and an aluminum foil window was provided in the heat shield.

D. Monitoring and Experimental Procedure

The primary monitor for the gamma-ray beam in this experiment was a thick-walled ionization chamber of the "Cornell" type. The beam was also monitored with a thin-walled chamber, but this was used only as a check on the other chamber. The walls of the "Cornell" chamber are 1-inch-thick copper. This construction makes the chamber preferentially sensitive to the high-energy portion of the bremsstrahlung spectrum, although still insensitive to the vast number of low-energy quanta or charged particles in the beam. The charge from the ionization chamber is collected on an integrating electrometer, which is accurate to better than 1%. An identical chamber has been calibrated at Cornell University in terms of the total energy content of the beam. This was done by two methods: one utilizing a pair spectrometer to measure the number of quanta in a given energy interval per microcoulomb integrated charge, the other utilizing a calorimetric method to measure directly the total energy in the beam.[20] The results of this calibration show there are 3.79×10^{12} Mev/microcoulomb at a peak bremsstrahlung energy of 340 Mev. Since some of

the discrepancies in the existing data may be due to calibrations of this type, we plan to do a recalibration in the near future, utilizing the 500-Mev linear accelerator at Stanford University. However, the existing calibration is used in the reduction of the data presented here.

In the morning of each running day the gain of each photomultiplier tube was checked with the small Ru^{106} sources, and the same was done at the time of shutdown at night. To minimize the effects of any electronic or accelerator drifts, data were taken at each angle many times, in a cyclic sequence, during the course of the experiment. Data with the target empty and the target full were taken in a cyclic sequence also.

III. RESULTS

A. Calculation of Cross Sections from Measured Counting Rates

1. General Considerations

In both the small-angle measurements and the angular-distribution measurements corrections were applied to the raw counting data to convert them into a differential cross section per incident photon. This involves finding the efficiency of the counter, and transforming the laboratory parameters associated with the counter telescope into quantities in the center-of-mass system. The latter may be called kinematical corrections. The kinematics of this reaction have been solved on the Illiac digital computer at the University of Illinois by Malmberg and Koester,[21] simplifying this aspect somewhat. The mean pion energy observed by the counter telescope at each angle was chosen to correspond to a fixed photon energy, and the laboratory-system angles were chosen to correspond to convenient angles in the center-of-mass system.

A general expression relating our observed counting rate to the differential cross section may be written

$$\frac{d\sigma}{d\Omega^*} = Y \cdot \frac{d\Omega}{d\Omega^*} \cdot \frac{1}{\Omega} \cdot \frac{1}{t} \cdot \left(\frac{\text{charge on ion chamber}}{\text{photon in accepted } \Delta E_\pi}\right) \cdot \frac{1}{\epsilon}$$

where

$\frac{d\sigma}{d\Omega^*}$ = center-of-mass system differential cross section, in square centimeters per incident photon per nucleon,

Y = number of counts per microcoulomb of charge integrated from the "Cornell" type ionization chamber,

$\frac{d\Omega}{d\Omega^*}$ = solid-angle transformation from the laboratory system of coordinates to the center-of-mass system of coordinates,

Ω = solid angle subtended by the telescope in the laboratory system,

t = thickness of the liquid hydrogen target, in hydrogen nuclei per square centimeter,

ϵ = efficiency of the counter telescope.

The π - μ telescope accepts a given ΔE_π which is a function of the mean pion energy in the laboratory system. The factor $\left(\frac{\text{charge on ion chamber}}{\text{photon in accepted } \Delta E_\pi}\right)$ is a measure of the charge in microcoulombs collected by the Cornell type ionization chamber per photon in the energy interval where it would be kinematically possible to produce a pion in ΔE_π. To compute this factor, the number of photons in a given photon energy interval must be calculated and related to the charge collected on the ionization chamber. Figure 12 is a plot of the Schiff thick-target bremsstrahlung spectrum for a peak photon energy of 340 Mev.[22] The area under this curve has the dimensions of energy, and is proportional to the total energy of the beam,

$$A = \int k\, N(k)dk \propto E_{total},$$

where k is the photon energy in Mev and N(k) is the number of photons per Mev at k energy. Now the fraction of the energy of the beam associated with photons in an energy interval Δk is just the ratio of the area under the curve in the increment Δk to the total area under the curve. If h is the height of the spectrum at k, then $\Delta k \cdot h/kA$ is the number of photons in Δk per Mev integrated beam, or

$$\frac{3.79 \times 10^{12}\, \Delta k \cdot h}{A \cdot k} = N(k, \Delta k) \text{ photons/}\mu\text{coulomb}$$

is the number of photons in Δk per microcoulomb integrated charge from the Cornell chamber, where the Cornell University calibration at a peak bremsstrahlung energy of 340 Mev, 3.79×10^{12} Mev/μcoulomb, has been used.

The kinematics of the reaction must now be utilized to determine the Δk of interest from the ΔE_π which is known for the telescope as a function of pion energy. The expression for this is

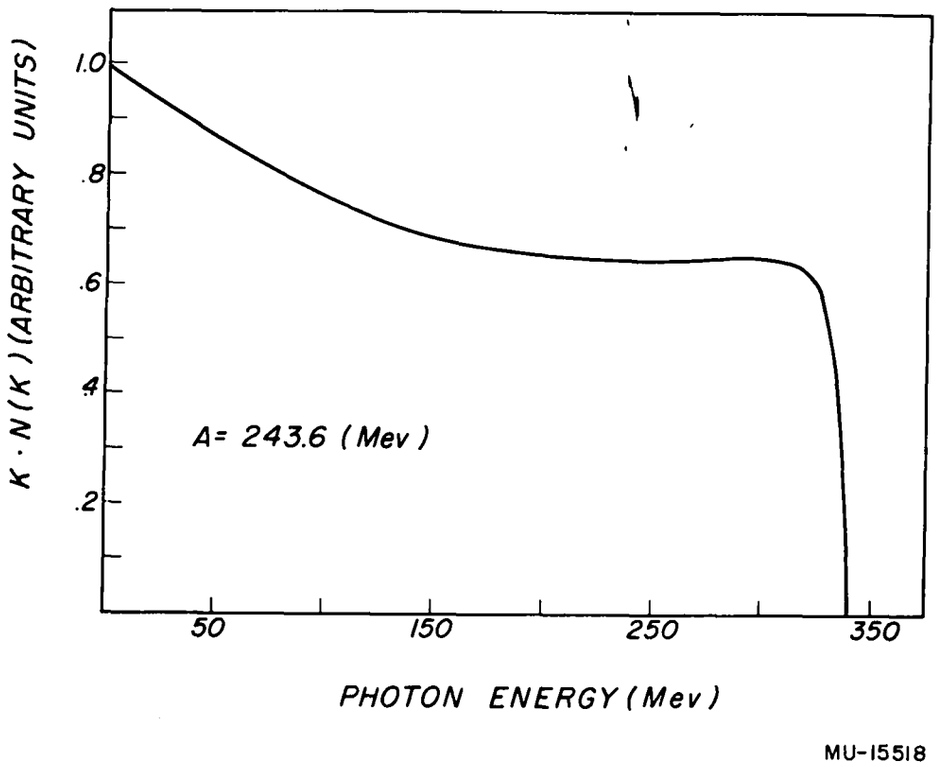

Fig. 12. Schiff thick-target bremsstrahlung spectrum. K_{max} = 340 Mev. The total area under the curve in units of Mev (normalization arbitrary) is indicated.

$$\Delta k = \left(\frac{dk}{dE_\pi}\right)_{\theta_{lab}} \Delta E_\pi \quad ,$$

where ΔE_π is the energy interval accepted by the telescope and

$$\left(\frac{dk}{dE_\pi}\right)_{\theta_{lab}}$$

may be evaluated from the kinematics of the reaction. Combining these factors one finds

$$\left(\frac{\text{charge on ion chamber}}{\text{photon in accepted } \Delta E_\pi}\right) = \frac{A}{3.74 \times 10^{12}} \cdot \frac{k}{h} \cdot \left(\frac{dE_\pi}{dk}\right)_{\theta_{lab}} \cdot \frac{1}{\Delta E_\pi} \cdot$$

In the wide-angle experiment all these quantities had to be evaluated in order to obtain the differential cross section. Since at the small angle the interest lies only in a relative angular distribution, only the energy or angle-dependent parts of this expression need to be evaluated. These are

$$\left(\frac{dE_\pi}{dk}\right)_{\theta_{lab}} \quad , \quad \Delta E_\pi \quad , \quad \frac{d\Omega}{d\Omega^*} \quad ,$$

and ϵ , the efficiency.

2. Kinematical Considerations

a. Wide-angle measurements

For the wide-angle telescope the kinematical considerations involve evaluating

$$\frac{d\Omega}{d\Omega^*} \quad , \quad \Omega, \quad t, \quad \left(\frac{dE_\pi}{dk}\right)_{\theta_{lab}} \quad , \text{ and } \Delta E_\pi \quad .$$

The solid-angle transformation was taken directly from the tables of Malmberg and Koester,[21] where it is evaluated explicitly for the cases which are of interest here.

$$\left(\frac{dE_\pi}{dk}\right)_{\theta_{lab}}$$

was evaluated by numerical differentiation of the kinematical tables. This function varies sufficiently slowly with photon energy to make this type of determination very accurate. The solid angle subtended in the laboratory system is defined by the area of the first counter in the telescope, and its distance from the target. Since the target has finite extension, changing angles will change slightly the effective solid angle seen by the telescope. This was investigated by a numerical integration, and found to be less than 0.5% between 30° and 90° (the solid angle at 30° and 150° is the same).

The effective thickness of the target was evaluated by integrating the size of the beam spot (1 inch in diameter) over the thickness of the cylindrical container. The diameter of this cylindrical Mylar vessel was known quite accurately (3.000 ± 0.02 in.) at room temperature, and the linear coefficient of expansion for Mylar was estimated and a correction was made for contraction upon cooling to liquid hydrogen temperatures. The value for this coefficient of expansion and for the density of liquid hydrogen (0.0708 g/cm^3) was taken from the Cyrogenic Data Book of the National Bureau of Standards.[23]

For a given telescope configuration the energy of the pion stopping in the center of the μ-meson scintillator (stopping scintillator) was computed by using the range-energy tables of Atkinson and Willis.[24] It is also possible to calculate the energy of π mesons that stop at the front and back edges of this scintillator, and the difference between these two energies is taken as the ΔE_π corresponding to the E_π that stops at the center. Figure 13 shows the results of this ΔE_π calculation. Some uncertainty is introduced into these computations because of edge effects in the stopping scintillator, but these may be estimated with good reliability. We estimate that ΔE_π is known to better than 1%.

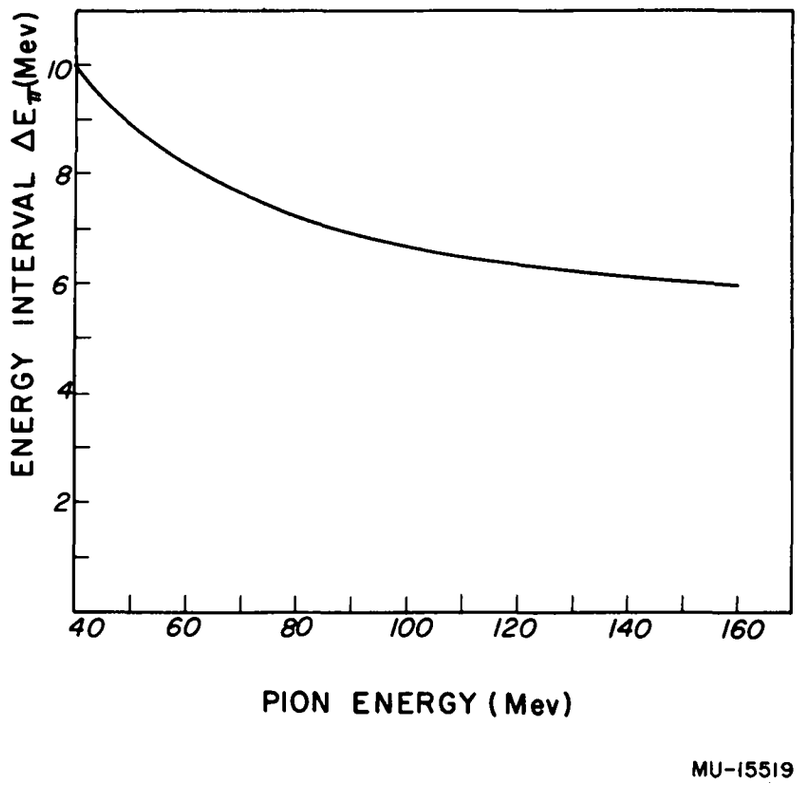

Fig. 13. Energy interval ΔE_π accepted by the wide-angle counter vs center pion energy.

b. Small-angle measurements

The quantities

$$\left(\frac{dE_\pi}{dk}\right)_\theta \quad , \quad \frac{d\Omega}{d\Omega^*} \quad , \text{ and } \quad \Delta E_\pi$$

were computed in the same manner for the small-angle telescope. If one defines the solid angle of the telescope as that subtended by the lead scatterer, this clearly stays fixed as angles are changed, and thus need not be evaluated for a relative measurement. The number lost by multiple scattering is discussed in the section dealing with counter efficiency.

3. Counter Efficiency

a. Wide-angle telescope

In order to know the efficiency of the $\pi - \mu$ telescope, one must determine the number of mesons lost because of the delayed-coincidence technique, and the number lost because of nuclear absorption and multiple scattering. The first of these is almost impossible to calculate from the electronic delay times, therefore an experiment was performed at the 184-inch cyclotron to determine the efficiency of the counter used in the wide-angle work. This calibration is discussed in detail in the Appendix, and the results are shown in Fig. 14.

The efficiency of the target telescope system is also affected by the multiple scattering of the mesons as they leave the hydrogen target and pass through the 3/32-in. aluminum vacuum tank wall. The aluminum wall is the major contributor to this effect, and it is sufficiently close to the solid-angle defining counter to make this correction negligible. Also, mesons decay in flight traveling from the target to the detectors. Since the flight path was quite short (about 18 inches), only a rough evaluation of this effect was made. The quantity

$$\left(1 - \frac{L}{\gamma\tau(\pi-\mu)\beta c}\right) = N/N_0$$

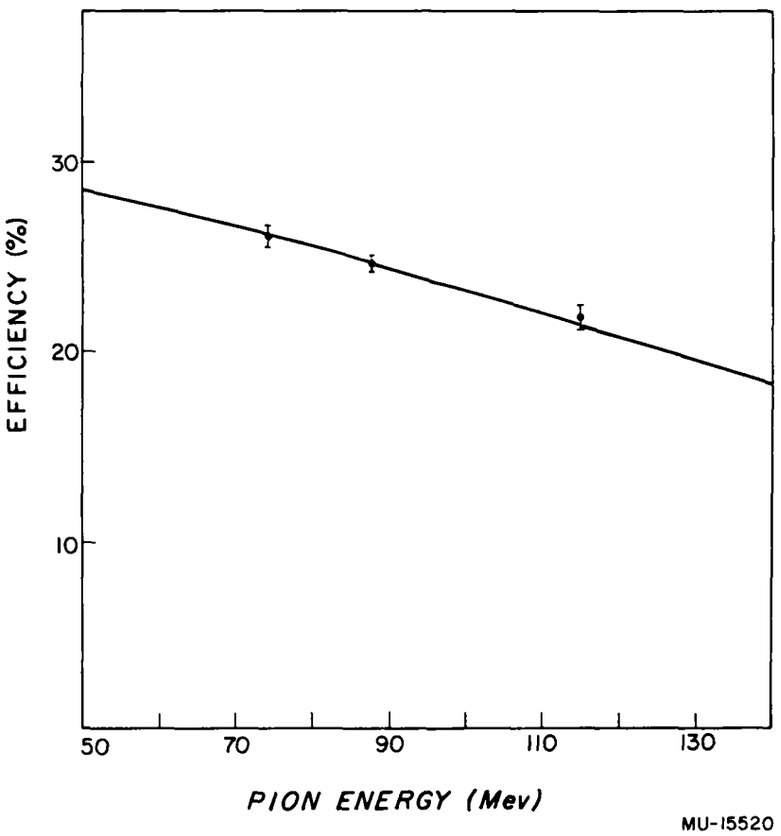

Fig. 14. Wide-angle counter efficiency as a function of pion energy from cyclotron calibration. The solid curve represents the calibration utilizing the half-life curve and the measured absorption cross sections, the experimental points represent the values obtained from the ratio of pions incident to pions counted. (See Appendix.)

was computed, where $\beta = v/c$, $\gamma = 1/\sqrt{1-\beta^2}$, L is the distance from the center of the μ-meson scintillator to the center of the target, $\tau(\pi-\mu)$ is the mean life for the decay of a π meson at rest, and N/N_0 is the fraction of those mesons starting that enter the telescope. This effect was not greater than 4% in any situation. The efficiency measured at the cyclotron was multiplied by this factor, evaluated as a function of energy before being applied to the raw data.

b. Small-angle telescope

The energy-dependent parts of the efficiency for the telescope are nuclear absorption of the pions in coming to rest in the stopping scintillator, and multiple Coulomb scattering in various parts of the channel or telescope. Any changes in geometry encountered when the angle of observation is changed also can change the relative efficiency.

For the case small-angle telescope, the corrections are all rather small, for the energy of the pions in the lab system changes only 15% in going from 0° to 40° observation angle at either photon energy. However, the situation is complicated by the lead channel and scatterer placed 10 inches from the scintillators. Because the pion-energy change is small and the gamma rays are close to the peak of the bremsstrahlung spectrum, the contribution due to higher-energy π mesons' being scattered from the walls of the channel into the correct energy band has been neglected. Estimates of the effect indicate it would be less than 5% of the total counting rate, and would not be sharply energy-dependent. Since there is no reason to expect the angular distribution of pions in this region to change radically from 260 Mev to the peak of the bremsstrahlung spectrum, the wall scattering probably affects the relative angular distribution less than 2%. The solid angle of the channel-telescope system is assumed to be constant in the laboratory system, for any angle of observation, and the angular acceptance of the channel is roughly the same as the size of the lead scatterer, for the scatterer spreads the meson beam out over an area about five times as great as the area of the stopping scintillator. As one changes angles, the effective width of the target

changes; and since the energy of the meson changes, the multiple scattering in the lead converter is different. A numerical evaluation of these effects was performed by tracing rays from various points in the target volume and numerically integrating the area under an appropriate multiple-scattering curve at the stopping scintillator. The results of this admittedly rough computation show that the effect can be no bigger than 1.5% between the two extreme angles, 0° and 40°, and is probably less. Thus this part of the efficiency dependence on energy was neglected.

The other energy-dependence part was the nuclear absorption of the mesons as they come to rest in the telescope. When the absorption cross section σ_A as a function of energy was known, the absorption correction was evaluated by finding the quantity

$$\epsilon = (1 - e^{-\int \sigma_A dx}) ,$$

where the integral in the exponent was taken through the various materials making up the counter telescope. This statement contains the implicit assumption that most of the diffraction-scattered mesons still come to rest in the stopping scintillator, or that the beam is sufficiently spread out so that roughly as many mesons scatter out as scatter in. In the small-angle telescope the latter is true, and the effect of leaving out the diffraction scattering has been neglected. The absorption cross sections were taken from Martin[25] and Stork.[26] The integral was evaluated numerically and the difference between the extreme cases is about 6 %. The effect of mesons decaying in flight is completely negligible, for the energies are nearly equal even in the extreme cases.

B. Final Results

Table I gives the final data in terms of the center-of-mass differential cross section,

$$\frac{d\sigma}{d\Omega^*} .$$

Table I'

Angular distribution of photopions from hydrogen			
260 Mev		290 Mev	
θ^*	$\frac{d\sigma}{d\Omega}^*$ (μ^b/sterad)	θ^*	$\frac{d\sigma}{d\Omega}^*$ (μ^b/sterad)
0	6.62 ± 0.65	0	6.90 ± 0.58
10	6.68 ± 1.13	10	7.16 ± 1.07
20	6.46 ± 0.76	20	7.62 ± 0.73
25	6.55 ± 0.87	30	6.96 ± 0.48
30	6.49 ± 0.51	40	9.23 ± 0.58
40	7.92 ± 0.49	50	11.90 ± 0.43
53	10.60 ± 0.50	70	15.90 ± 0.51
70	15.35 ± 0.39	90	19.86 ± 0.46
90	17.59 ± 0.47	115	19.50 ± 0.54
115	17.88 ± 0.37	140	16.72 ± 0.40
140	17.60 ± 0.34	160	13.76 ± 0.59
160	16.47 ± 0.38		
σ_{total} = 185 ± 13.5 microbarns		σ_{total} = 199 ± 14 microbarns	

The small-angle region has been normalized to the backward-angle portion by a weighted average of the three normalizing coefficients obtained at each energy from the data in the region of overlap. Also in this region the measurements have been combined to give one point at each angle. In no case were these points separated by more than 1 standard deviation after normalization. The normalization error has been propagated to the forward points.

The counting statistics are probably the greatest source of error in the angular dependence of the cross section, and the standard deviation due to these is quoted with the data. The reasons

for this belief have been enumerated in the preceding section. However, the counting statistics may not be the largest error associated with the absolute value of our measurements; additional uncertainty arises from the calibration of the Cornell ionization chamber and there are uncertainties in the absolute efficiency of the wide-angle telescope. Thus the total cross section, obtained by integrating our differential measurements, is quoted to 7% accuracy, although the integral is good to better than 4% statistically. This is a quite liberal allowance for systematic error, barring a very large error in the Cornell-chamber calibration.

The data are presented graphically with the rest of the available data from other laboratories in Figs. 15 and 16.

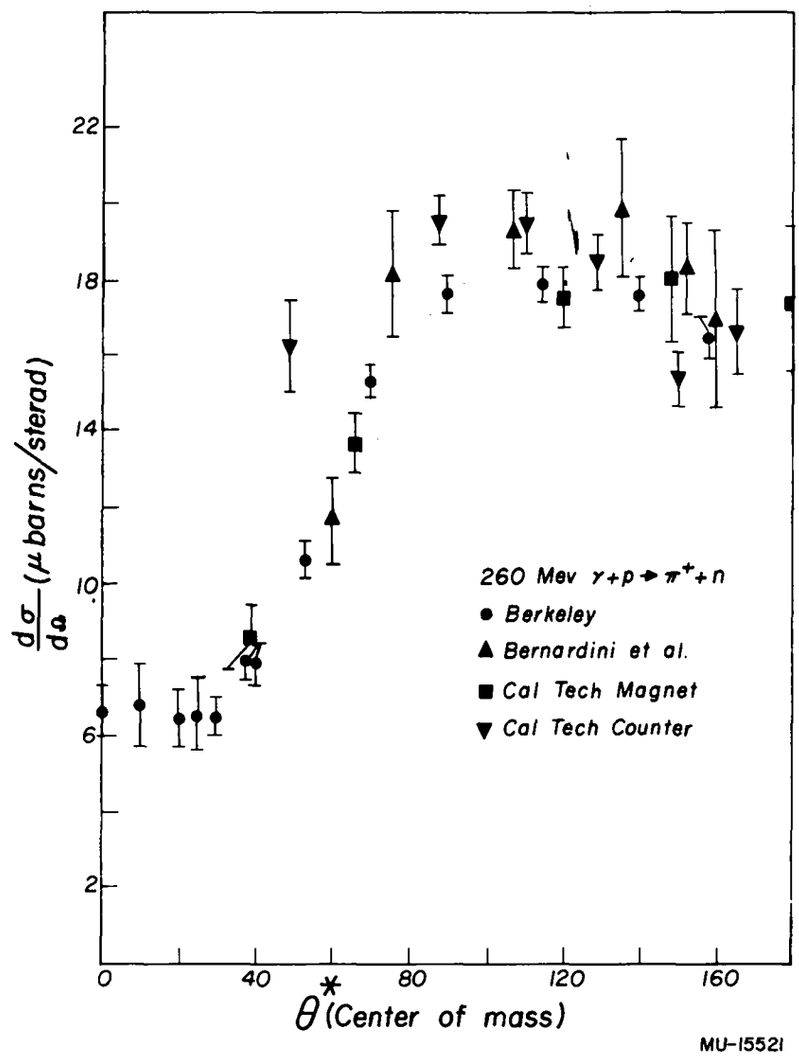

Fig. 15. The differential cross section for positive photopion production from hydrogen at a photon energy of 260 Mev. Superimposed on the data reported here are the results of the magnet[6] and counter[7] groups' determinations at the California Institute of Technology, and the data taken from Bernardini's compilation.[8]

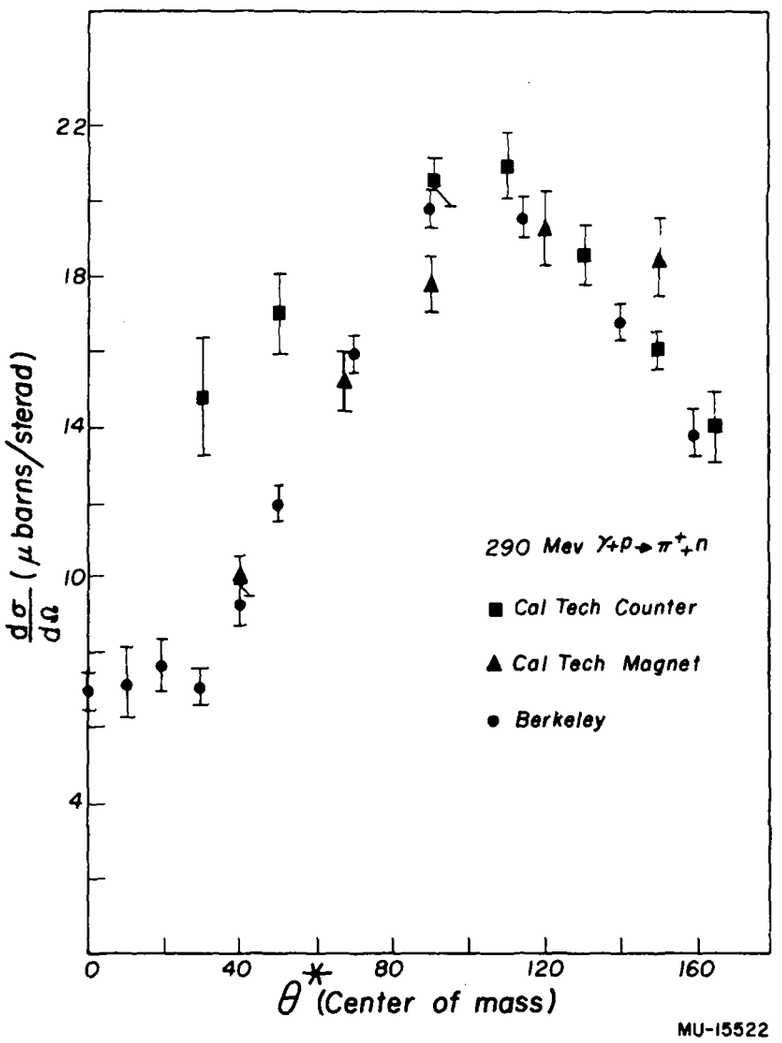

Fig. 16. The differential cross section for positive photopion production from hydrogen at a photon energy of 290 Mev. Superimposed on the data reported here are the results of the magnet[6] and counter[7] groups' determinations at the California Institute of Technology.

IV. DISCUSSION

A. Analysis of the Data by the Moravcsik Method

In previous analyses of experimental measurements on the photoproduction of positive pions,[10, 27] it had been customary to express the differential cross section in terms of a quadratic in $\cos\theta^*$, e.g.,

$$\frac{d\sigma}{d\Omega^*} = A + B\cos\theta^* + C\cos^2\theta^* ,$$

where the assumption is made that at low energies only S- and P-wave mesons contribute in the final state. Moravcsik has pointed out that for charged mesons this expansion is not valid, for the photon can interact not only with the nucleon but also with the charged pion cloud surrounding the nucleon. This interaction is of the form

$$\int \vec{j}_\pi \cdot \vec{A}\, d\tau \propto \frac{(\vec{\epsilon}\cdot\vec{q})\,\vec{\sigma}\cdot(\vec{k}-\vec{q})}{q_0 k - \vec{q}\cdot\vec{k}} ,$$

where $\vec{k}$ and $\vec{\epsilon}$ are the photon momentum and polarization, $\vec{q}$ and q_0 are the momentum and energy of the meson, and $\vec{\sigma}$ is the nucleon spin. The denominator of this expression may also be written $(1-\beta\cos\theta^*)\cdot q_0 k$ where again θ^* is the pion emission angle and β the meson velocity, in the center-of-mass system. This expression introduces all higher angular-momentum states and thus invalidates the quadratic expression, for the expansion of $(1-\beta\cos\theta^*)^{-1}$ is an infinite series in $\cos\theta^*$. For a photon energy of 260 Mev we have $\beta = 0.756$ and for 290 Mev $\beta = 0.800$. Because these values of β are reasonably large, this term can be quite important in the cross section in the forward-angle region, where $(1-\beta\cos\theta^*)$ becomes small. This entire process is in many ways analogous to the ejection of electrons from atoms by the photoelectric effect, and the cross section for this effect has a similar denominator. This denominator is of relativistic origin, arising from the retardation effects in the meson current potential.

To take this process into account, Moravcsik has suggested analyzing the angular distribution of the charged photopions by an

expression of the form

$$\frac{d\sigma}{d\Omega^*} = \sum_{n=0}^{4} \frac{A_n \cos^n \theta^*}{(1-\beta \cos \theta^*)^2} \quad ,$$

where the A_n are to be determined by a least-squares fit to the data. This least-squares fit has been performed for our data at 260 and 290 Mev, and the curve representing this expansion is shown superimposed on our data in Figs. 17 and 18. The values obtained for the A_n are given in Table II.

Table II

Moravcsik coefficients determined by least-squares fitting

k (Mev)	A_0	A_1	A_2	A_3	A_4
260	17.511	-31.117	9.356	6.433	-1.765
290	19.638	-36.799	9.083	16.373	-8.014

Quantities of physical interest, such as multiple-production amplitudes , are not simply related to these coefficients. However, the curve these coefficients represents is useful, for it is of the same form as predicted by theory and may be used in the comparison of experimental data with theoretical predictions. The abrupt flattening of the experimental cross section in the forward direction may be explained by the existence of the "photoelectric" term in the theoretical expressions. This behavior would not be expected if this interaction were absent, such as in π^0 photoproduction.

B. Comparison with Theory

The theory of photomeson production at present believed to be the most accurate is that derived from the dispersion relations for the photoproduction amplitude by Chew, Goldberger, Low, and Nambu.[12] (No detailed description of this theory is presented here.)

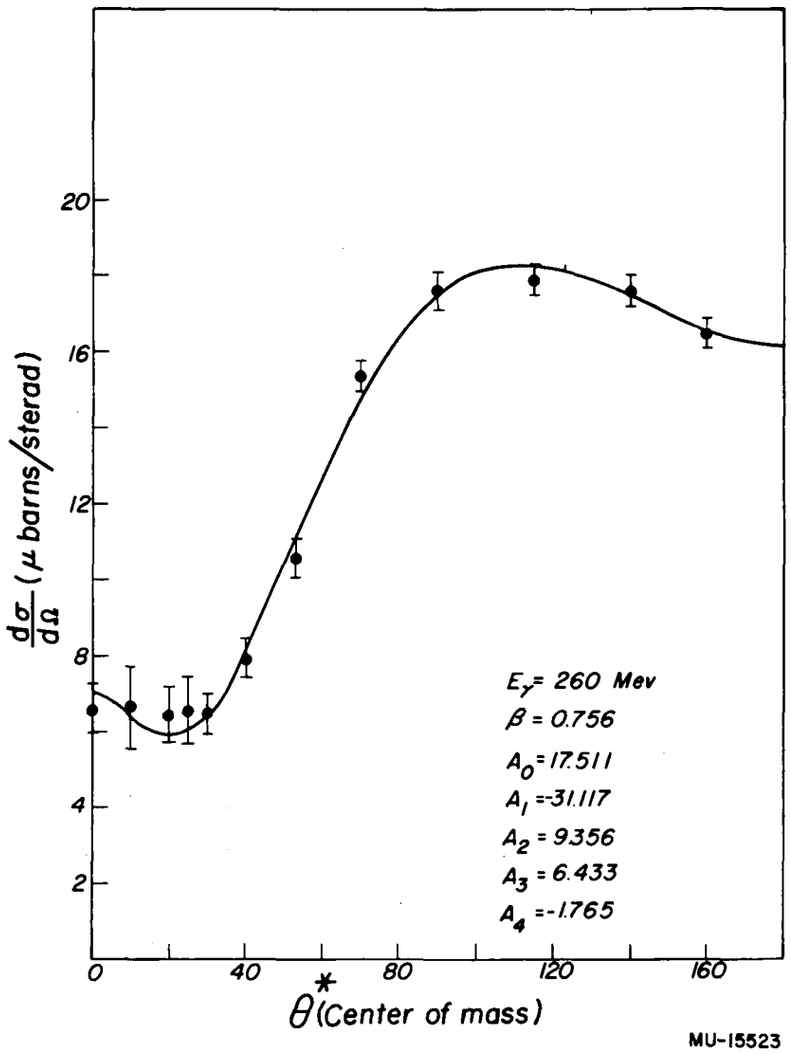

Fig. 17. Differential cross section for positive photopion production from hydrogen at 260 Mev. The solid curve represents the Moravcsik fit to the data.

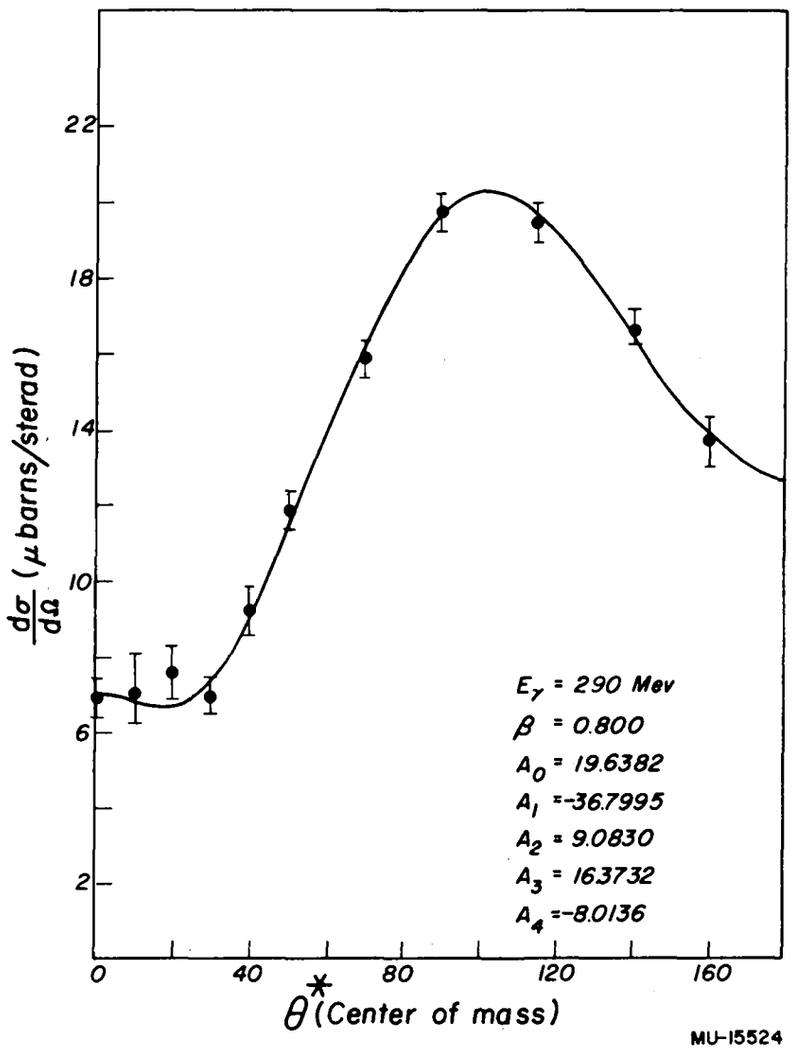

Fig. 18. Differential cross section for positive photopion production from hydrogen at 290 Mev. The solid curve represents the Moravcsik fit to the data.

The dispersion relation here used is an integral expression relating the real and imaginary parts of the photoproduction amplitude, and is derived by using very general considerations. Chew, Goldberger, Low, and Nambu integrate this dispersion relation, making various assumptions that simplify the problem sufficiently to allow the computation to be performed. These assumptions include neglect of all terms of order v^2 in the nucleon velocity. In the energy region where these measurements have been made, the error introduced by dropping these terms amounts to about 10%, and the theory should not be expected to describe the process more accurately than this.

In the process of evaluating the dispersion integrals, use is made of the unitarity of the S matrix to relate parts of the photomeson amplitudes to quantities which are known, in this case the pion-nucleon scattering amplitudes. The input data in the theory thus contain the pion-nucleon scattering phase shifts in addition to the pion-nucleon coupling constant, the electronic charge, and the magnetic moments of the proton and neutron.

The expressions derived by Chew, Goldberger, Low, and Nambu have been recently evaluated by Uretsky,[28] using various assumptions about the small pion-nucleon phase shifts that enter the evaluation but are not well known experimentally. In Uretsky's initial calculations the P-wave phase shifts were computed from the effective range relations of Chew, Goldberger, Low, and Nambu,[29] and the S-wave phase shifts were taken to obey the relation

$$2\delta_1 + \delta_3 = 0.229\, q\,,$$

which is suggested by Orear's analysis.[30] This choice is a reasonable one according to the existing analysis of pion-nucleon scattering data, and the results are shown by the heavy line in Figs. 19 and 20.

In order to determine how sensitive the theory was to the choice of these small phase shifts, Uretsky then made three changes. First, he set δ_{11} to zero. The results here were incompatible with the experimental data presented, for the cross section became very

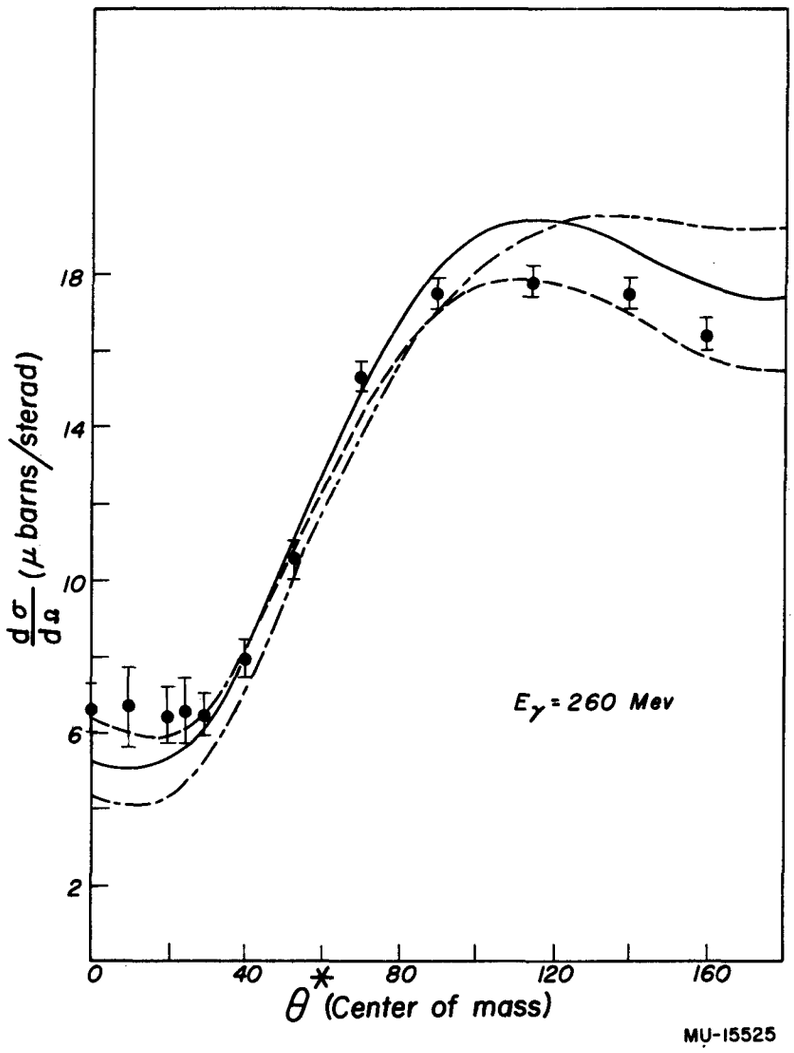

Fig. 19. Differential cross section for positive photopion production from hydrogen at 260 Mev. For an explanation of the curves see the text.

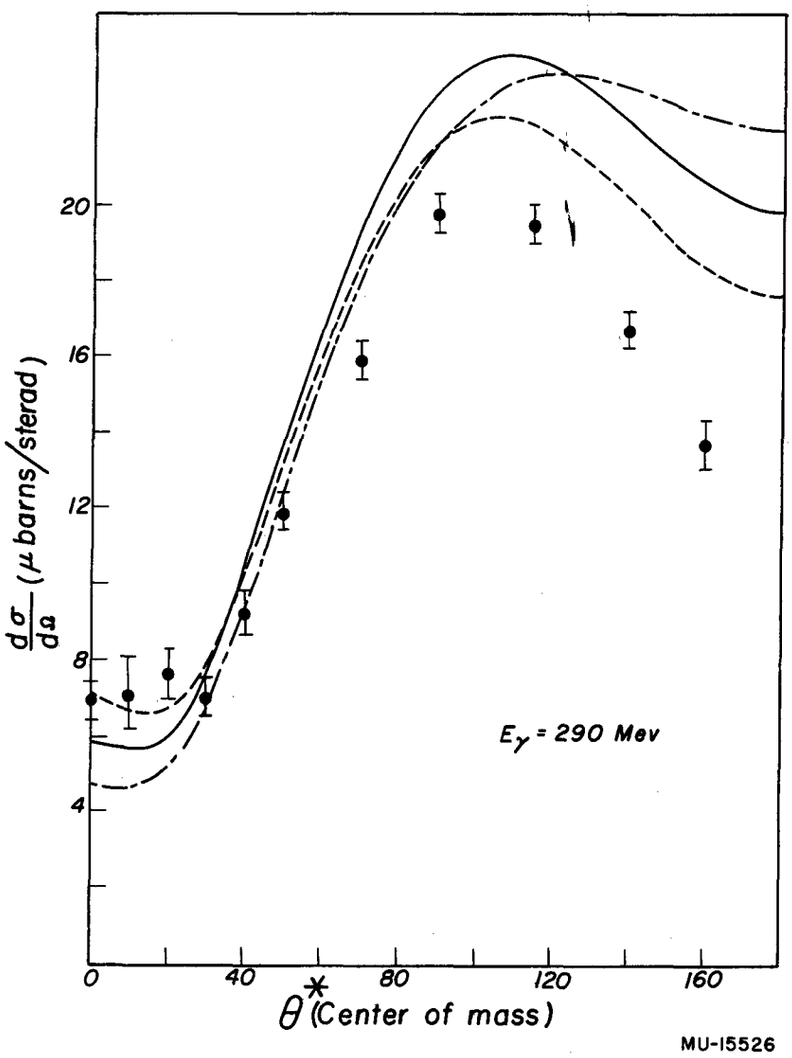

Fig. 20. Differential cross section for positive photopion production from hydrogen at 290 Mev. For an explanation of the curves see the text.

large at the backward angles. Secondly, he set δ_{31} and δ_{13} equal to zero, leaving the other parameters unchanged. The results of this computation are shown by the dotted lines in Figs. 19 and 20. Lastly, he used Anderson's formulae for the phase shifts δ_{11}, δ_{31} and δ_{13},[31] with the result shown by the "dash-dot" curves in Figs. 19 and 20. Comparison of these predictions to the experimental points shows that the choice $\delta_{31} = \delta_{13} = 0$ yields the best fit to the data in both cases.

The results of Uretsky's computations are surprisingly sensitive to the choice of these small phase shifts, which are not known very accurately. However, the photoproduction data probably cannot be used at this time to determine the values of these small phase shifts, which are very difficult to measure in pion-nucleon scattering experiments owing to the predominance of the well-known "3, 3" phase shift at these energies. This hesitation arises in part from the 10% error in the theoretical expression due to the assumptions made in its derivation, and in part from the large number of parameters free to adjust, that is, all the phase shifts. The verification of the theoretical differential cross section must therefore await more accurate determinations of the small pion-nucleon phase shifts.

C. Conclusions

The behavior of the measured differential cross section in the region from 0° to 40° clearly shows the effects of the "photoelectric" term in the theoretical differential cross section. When a comparison is made to the dispersion-relations theory of Chew, Goldberger, Low, and Nambu,[12] the theory describes the measurements very well at 260 Mev and somewhat less accurately at 290 Mev, if δ_{13} and δ_{31} are set equal to zero. No particular significance is attached to this choice of phase shifts, however, for the theory has assumptions that may affect the predictions by more than 10%, and the number of

combinations of phase-shift choices is very large. However, the gross details of the measurements are certainly reproduced by the theoretical curves.

ACKNOWLEDGMENTS

I wish to express my appreciation to the many people who have been of such great help during the course of this experiment. I would especially like to thank Professor A. C. Helmholz for his guidance throughout my graduate work. I am very grateful to Drs. Robert Kenney and Victor Perez-Mendez for their physical and moral support in the planning and execution of this experiment, and to Dr. William Imhof for his support in the early phases of the work. Thanks are also due Mr. Walton Perkins and Mr. John Caris for their assistance in the execution of the experiment.

Finally, I wish to thank Mr. Rudin Johnson and the synchrotron crew, and Mr. James Vale and the cyclotron crew for their assistance and cooperation during the course of the experimental work.

This work was done under the auspices of the U. S. Atomic Energy Commission.

APPENDIX

Wide-Angle Counter Calibration at the 184-Inch Cyclotron

The efficiency of the π-μ telescope used in the experiment was determined at the 184-inch cyclotron by two independent methods. Both methods made use of a "clean" pion beam which was extracted into the meson cave. In the first method, the efficiency due to the delayed coincidence was determined from a half-life curve, and then the known absorption cross sections were utilized to determine the total efficiency as a function of pion energy. In the second method, the ratio of pions detected by π-μ decay to the total number of incident pions was measured at three energies, giving the efficiency directly without resort to any other experimental quantities. These two methods agree very well, as is seen below.

An internal target was used to produce the meson beam as shown in Fig. 21. A remotely controlled carbon target inside the cyclotron vacuum tank was struck by 730-Mev protons, and the π mesons produced at some backward angle were deflected out of the magnetic field and into an 8-foot collimator. Since it was important to have the beam as monoenergetic as possible, a secondary bending magnet was utilized to give better energy resolution. The beam was collimated again directly in front of the counter to 4 by 4 inches by a 4-foot iron collimator. The energy of the beam was changed by changing the position of the target inside the cyclotron and varying the current in the secondary bending magnet. Three energies, 72, 87.5, and 115 Mev, were used. The beam consisted of pions, muons from π-μ decay, and some electrons. For the flux of incident pions to be estimated, the fractions of each of these constituents must be measured. This was accomplished with the use of a range curve, such as is shown in Fig. 22. The electronics used to obtain these results are shown in Fig. 23a. The three scintillators were 6 by 6 inches, 0.5 inch thick, and were each viewed by one RCA 6810-A photomultiplier tube. A double coincidence between the first two

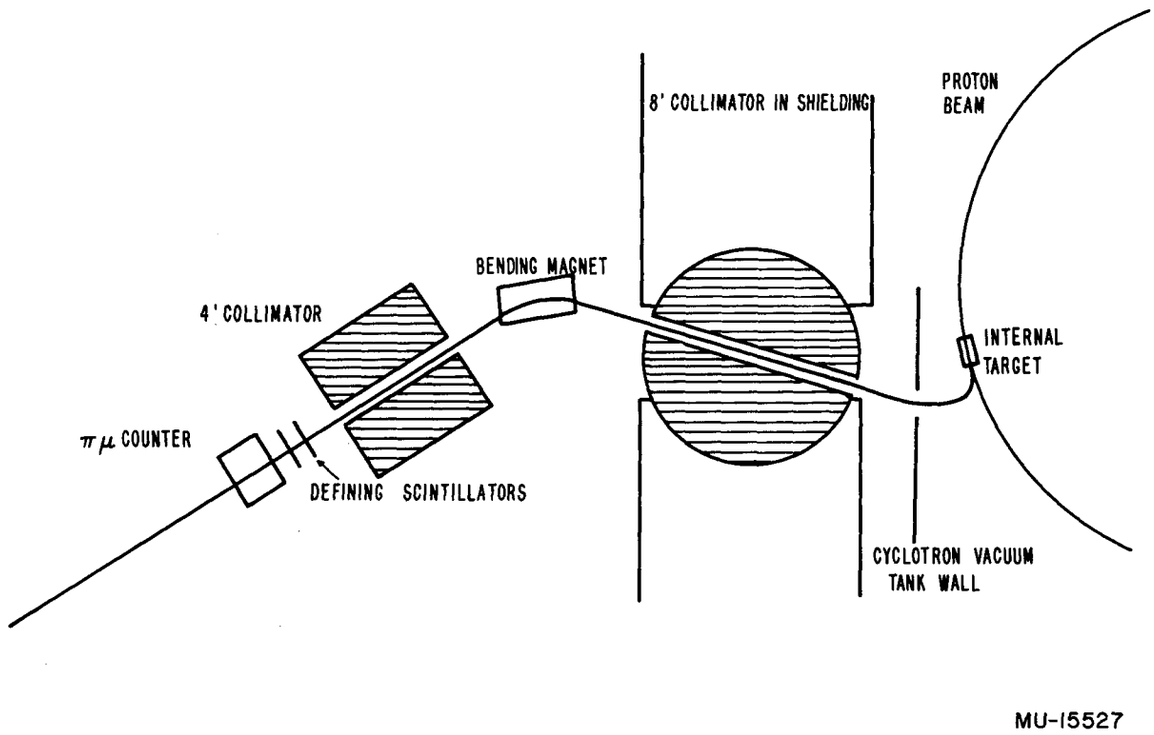

Fig. 21. Arrangement of experimental apparatus at the 184-inch cyclotron for the calibration of the $\pi - \mu$ telescope.

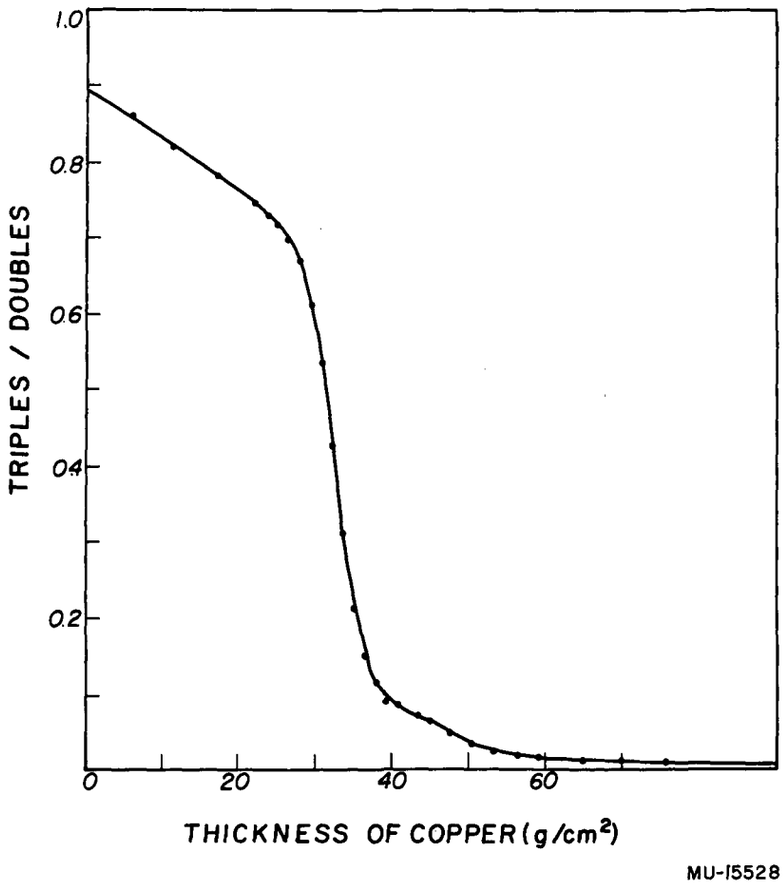

Fig. 22. Range curve in cyclotron pion beam. E_{π} = 87 Mev.

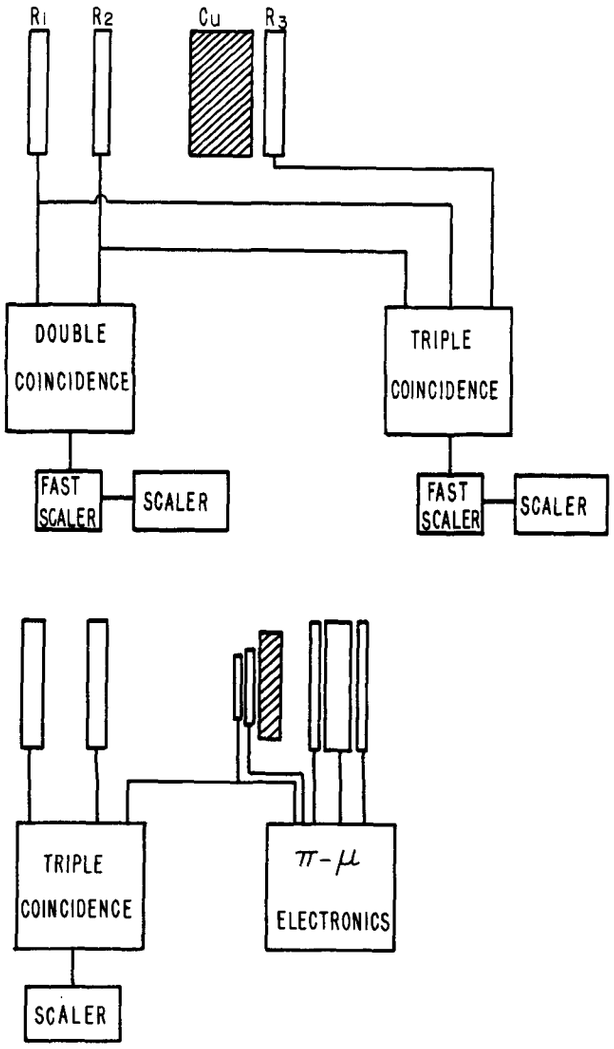

Fig. 23a. Block diagram of the electronics used in the range measurements.

23b. Block diagram of electronics used in π - μ telescope calibration.

counters recorded the total number of particles entering the telescope. Copper was placed between these two scintillators and the third scintillator, and a triple coincidence recorded the number of particles passing through the whole telescope. As the amount of copper was increased, first the pions stopped, then the muons of the same momentum, and finally only the electrons were left. This behavior is shown in Fig. 22. The number of pions in the beam may be estimated with good accuracy from a curve of this type; or better, a differential range curve may be obtained by numerical differentiation of this curve and the number of muons determined from this. The differential range curve obtained from the 87-Mev range curve is shown in Fig. 24. The electron contamination is more difficult to determine, but fortunately it was small. The energy of the beam was determined by the range of the pions.

With the constituents of the beam known, the copper and last scintillator were removed and the π-μ telescope substituted. In this case the number of incident particles was determined by a triple coincidence between the first two scintillators, as used in the range measurement, and the first counter of the π-μ telescope. The electronics for this arrangement are shown in Fig. 23b. The π-μ counting equipment and cables were identical to those used at the synchrotron except for the cables that led to the counting room from the radiation area. These cables are known to be of the same electrical length to $\frac{1}{4}$ inch at both the cyclotron and synchrotron.

First, the efficiency due to the delayed coincidence alone was measured. It is possible to find a point of the differential range curve where almost 100% of the particles stopping are pions. Copper absorber was placed in the π-μ telescope so that pions of this energy stopped in the center of the stopping scintillator. Then a half-life curve was taken, by varying the delay of the delayed gate. This curve is shown in Fig. 25. If only pions stop in the scintillator and the anticoincidence counter rejects all particles that pass into it, the

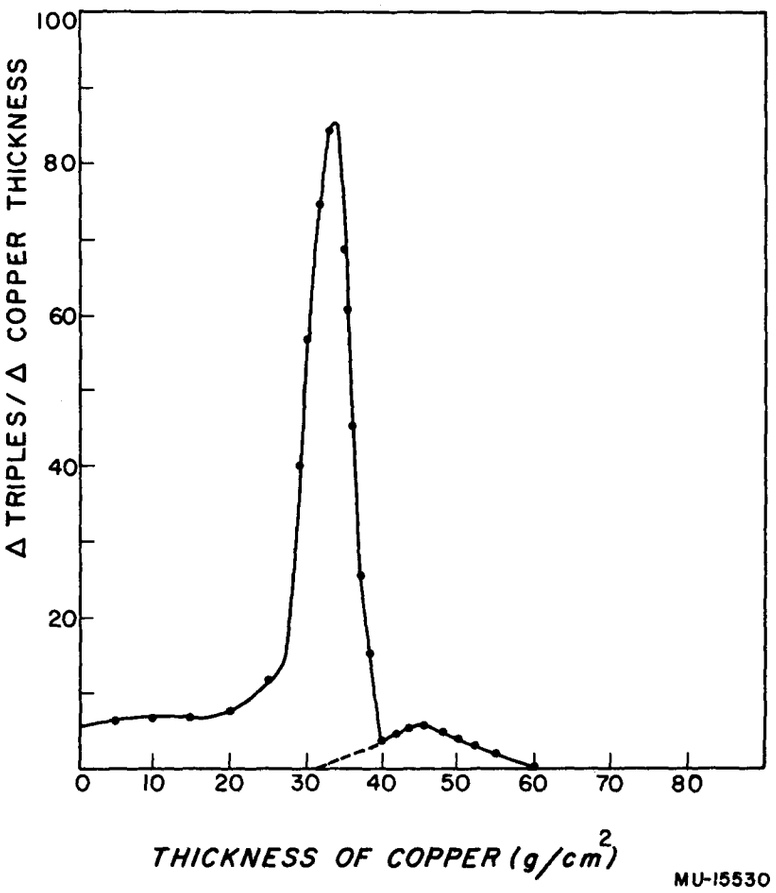

Fig. 24. Differential range curve for 87-Mev pions.

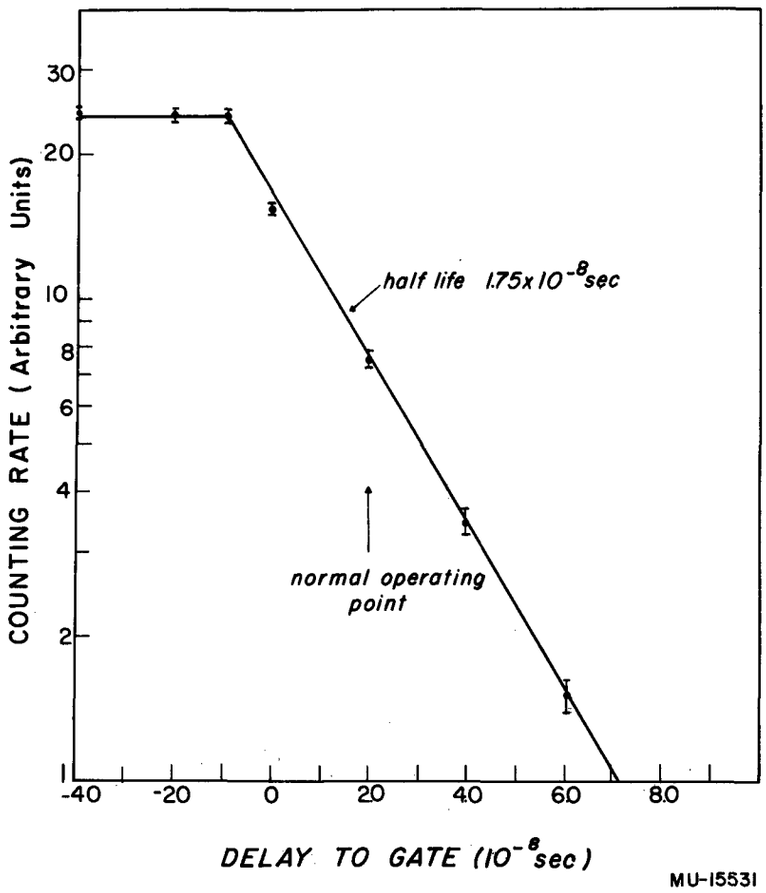

Fig. 25. Half-life curve taken at cyclotron.

ratio of the plateau height of the curve to the height where the electronics are normally operated gives the efficiency due to the delayed coincidence. The total efficiency may then be determined by calculating the loss due to multiple scattering and absorption, utilizing the known experimental cross sections. The counter was originally designed so that the correction due to multiple scattering would be negligible. The loss due to absorption was calculated by evaluating the quantity $\epsilon = (1-e^{-\int \sigma A dx})$, where the integral is taken through the various materials in the telescope. This is completely analogous to the calculation made for the small-angle telescope, and the same experimental cross sections were used here.[25, 26] Since most of the diffraction scattering occurs close enough to the stopping scintillator to be contained by it, any loss due to this was neglected.

The efficiency was also determined in a completely independent way by finding the ratio of incident pions to those counted by π- μ decay. The energy spread of the incident beam was comparable to, or a little larger than, the energy interval accepted by the telescope. For this reason, the energy accepted by the telescope had to be varied so that all pions incident on the telescope would be taken into account. The curve obtained when this was done is shown in Fig. 26. The ordinate of this curve is $N(E, \Delta E)$, the number of pions stopping in ΔE centered at E. Then the total number of pions stopping and being counted is

$$N = \sum_{n=0}^{(E_1+n\Delta E)\geq E_2} N[(E_1 + n\Delta E)_1 \Delta E] ,$$

where E_1 and E_2 define the limits of the pion energy interval in the beam and ΔE is the energy interval accepted by the telescope. The curve for $N(E, \Delta E)$ shown in Fig. 26 has a histogram superimposed upon it showing this summation. The efficiency is then the ratio of this sum to the number of incident pions as determined from the range curve.

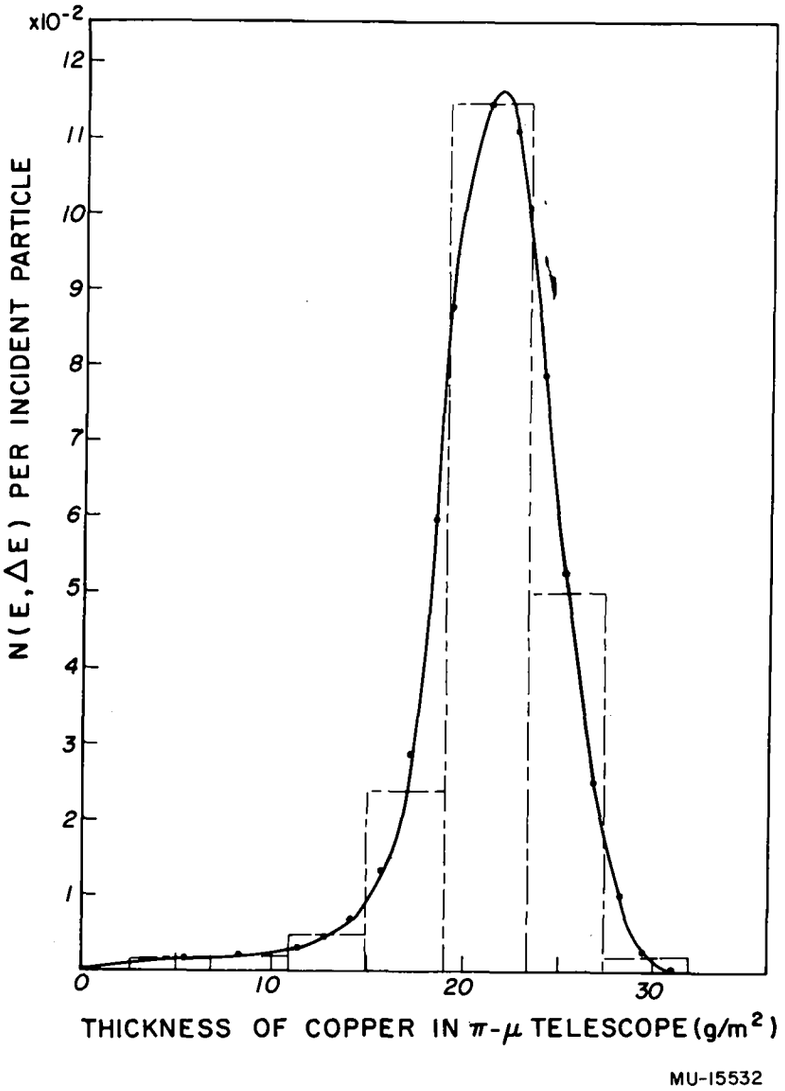

Fig. 26. Curve of N(E, ΔE) vs thickness of copper absorber in the telescope. See explanation in text.

The results of these two methods are shown in Fig. 14 (presented earlier). The solid curve is the efficiency determined by integrating the known experimental cross sections and utilizing the efficiency determined by the half-life curve. The three experimental points are estimates of any error involved in determining the fraction of pions in the beam and the uncertainty in the equality of cable lengths leading from the radiation area to the counting room. They are not statistical in nature. The two methods, even though quite different in principle, agree very well.

REFERENCES

1. J. Steinberger and S. A. Bishop, Phys. Rev. 86, 171 (1952,
2. White, Jacobsen, and Schulz, Phys. Rev. 88, 836 (1952).
3. Jarmie, Repp, and White, Phys. Rev. 91, 1023L (1953).
4. G. Bernardini and E. L. Goldwasser, Phys. Rev. 94, 729L (1954).
5. Jenkins, Luckey, Palfrey, and Wilson, Phys. Rev. 95, 179 (1954).
6. Walker, Teasdale, Peterson, and Vette, Phys. Rev. 99, 210 (1955).
7. Tollestrup, Keck, and Worlock, Phys. Rev. 99, 210 (1955).
8. Beneventano, Bernardini, Carlson-Lee, Stoppini, and Tau, Nuovo cimento, Series 10, 4, 323 (1956).
9. L. S. Osborne and B. Richter in Proc. Annual Rochester Conf. High-Energy Nuclear Physics 6 (Interscience, New York, 1956), Sec I, p. 25.
10. Watson, Keck, Tollestrup, and Walker, Phys. Rev. 101, 1159 (1956).
11. G. F. Chew and F. E. Low, Phys. Rev. 101, 1579 (1956).
12. Chew, Goldberger, Low, and Nambu, Phys. Rev. 106, 1345 (1957).
13. M. J. Moravcsik, Phys. Rev. 104, 1451 (1956).
14. A. Lazarus, Stanford, private communication.
15. J. H. Malmberg and C. S. Robinson, Phys. Rev. 109, 158 (1958).
16. Chamberlain, Mozley, Steinberger, and Wiegand, Phys. Rev. 79, 394 (1950).
17. Imhof, Kalibjian, and Perez-Mendez, Rev. Sci. Instr. 29, 476 (1958).
18. F. Evans, UCRL Counting Handbook (unpublished).
19. H. A. Bethe and F. de Hoffman, Mesons and Fields, Vol. II (Row, Peterson, Evanston, Ill. 1955).
20. Robert R. Wilson, Cornell private communication to Robert W. Kenney.
21. J. H. Malmberg and , L. J. Koester, Jr., "Tables of Nuclear Reaction Kinematics at Relativistic Energies," privately circulated tables, University of Illinois, Physics Research Laboratory, 1953.
22. L. I. Schiff, Phys. Rev. 83, 252 (1951). Calculation by Larry Higgins, UCRL, private communication.

23. D. B. Chelton and D. B. Mann, Cryogenic Data Book, UCRL-3421 May 1956.
24. John H. Atkinson, Jr. and Beverly Hill Willis, "High-Energy Particle Data," UCRL-2426 (revised), Vol. II, June 1957.
25. R. Martin, Phys. Rev. 87, 1052 (1952).
26. D. Stork, Phys. Rev. 93, 868 (1954).
27. K. A. Brueckner and K. M. Watson, Phys. Rev. 86, 923 (1952).
28. J. L. Uretsky, R. W. Kenney, E. A. Knapp, and V. Perez-Mendez, Photoproduction of Positive Pions from Protons (submitted to Physical Review).
29. G. F. Chew, M. L. Goldberger, F. E. Low, and Y. Nambu, Phys. Rev. 106, 1337 (1957).
30. J. Orear, Nuovo cimento 4, 856 (1957).
31. Anderson in Proc. Annual 1956 Rochester Conf. High-Energy Nuclear Physics 6 (Interscience, New York, 1956), Sec. I, p. 20.